Tensile resistance of bolted angle connections in the beam-column joint against progressive collapse

Ying Zhang[1], Jingxuan Wang[2], Shan Gao[3,4*], Sheliang Wang[1], Feng Fu[5]

1. School of Civil Engineering, Xi'an University of Architecture and Technology, Xi'an 710123, China

2. School of Civil Engineering, Lanzhou University of Technology, Lanzhou 730050, China

3. Shaanxi Key Laboratory of safety and durability of concrete structures, Xijing University, Xi'an 710123, China

4. Postdoctoral Station of Civil Engineering, Chongqing University, Chongqing, China

5. School of Mathematics, Computer Science & Engineering, City, University of London, London, EC1V0HB, UK

Abstract: In this paper, an experimental study was carried out on the bolted angle connection under uniaxial tension. The design parameters of the tested connections include angle thickness, bolt hole distribution, bolt diameter and bolt preload. In total 20 specimens were tested with five different kinds of failure modes observed. The experimental results showed that angle thickness, horizontal bolt pitch and vertical bolt pitch all affect the failure modes of the connections and are positively correlated with their ultimate bearing capacity. Significant plastic deformation appeared in both the horizontal and vertical legs of the angle. Based on the experimental results and the corresponding theoretical analysis, a mechanical model of bolted angle connection is proposed to predict its initial stiffness, ultimate bearing capacity and ultimate deformation and verified against the tested results and other mechanical models, in terms of uniaxial tensile load-displacement curves. The proposed model fits with the tested results better than other models.

Keywords: Bolted angle connection; Bolt preload; Tensile behavior; Mechanical model; Progressive collapse

1. Introduction

For decades, the analysis and design of progressive collapse of structures has become a research hotspot [1]. The reason for triggering the progressive collapse of a structure may be due to the sudden failure of the partial vertical supporting components under the accidental load such as explosion and terrorist attack. Sudden failure of partial supporting components can produce dynamic effect on the surrounding structural and non-structural components whilst the internal force on the structure would be redistributed to the horizontal component connected to the damaged vertical supporting components through the joints between them [2-3]. Through experiment and numerical simulation, the anti-collapse performances of the frame structures in the scenario of column removal were studied, involving concrete frame [4-7], steel frame [8-11], composite frames [12-15].

Preventing progressive collapse of buildings has been also recognized as an important design consideration, for both quantitative and qualitative design. A series of design standards have been published across the world, such as British Standard [16], Eurocode [17], NBCC [18], GSA [19], and DoD [20], involving two design methods known as "direct design" focusing on quantitative performance of structures and "indirect design" tending to prevent progressive collapse in the perspective of qualitative performance.

In all above design guidelines, beam-column joints play a crucial role for the internal force redistribution. Their performance will directly affect the strength, stiffness and stability of the whole structure. At present, the commonly used connection forms in prefabricated steel structures mainly invovles end-plate connections, bolted angle connections, fin-plate connections and so on [21-22]. Bolted angle connections exhibht strong energy dissipation capacity and excellent deformation capacity under large deflection [23-25]. Therefore bolted angle connection is supposed to be a preferable configuration in the anti-collapse design for prefabricated steel structures. The experimental and simulation studies both show that the strength and deformation capacity of bolted angle connection under proper design could meet the requirement against progressive collapse resulting from single column loss [26-30].

As Component Method in Eurocode 3 stipulates [31], T-stub is a basic but key component in bolted steel beam-column joints as shown in Fig. 1. After assembled from various components, the mechanical performance of bolted beam-column joints including resistance and initial stiffness could be predicted by using Component Method. Since normally T-stub is considered as a tensile component in bolted beam-column joint, several tests and simulations were conducted on the deformation and resistance capacity of the T-stubs under uniaxial tension, regarding the dimension of T-stub and bolt distribution[32-36]. In addition, it should

be mentioned that in some cases, the T-stub connecting beam web and column flange is acturally under the combination of tension and shear load, which is not covered by Component Method in Eurocode 3.

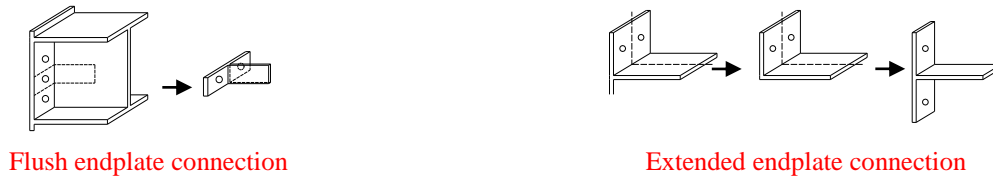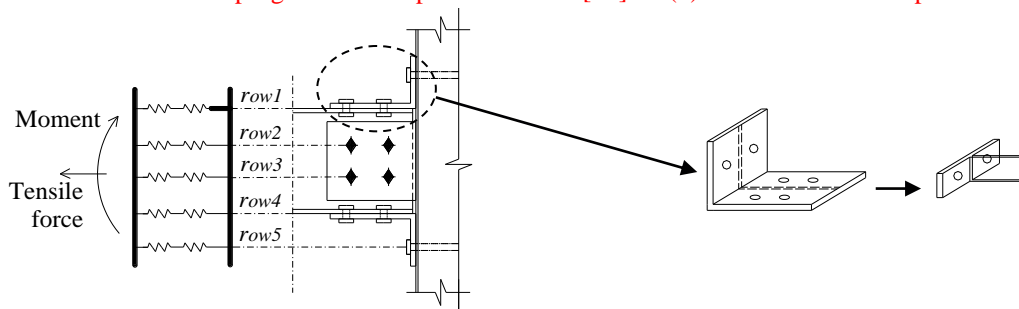Flush endplate connection   Extended endplate connection
Fig. 1 T-stub in bolted steel connections

As shown in Fig. 2(a), to predict the full vertical load-deformation relationship of the sub-structure against progressive collapse which is simplified from a whole structure, the mechanical performance of the beam-column joint needs to be known, as shown in Fig. 2(b). Subsequently, the beam-column joint could be represented by various components basend on Component Method in Eurocode 3 as shown in Fig. 2(c) where the full load-deformation relationship of each component is required. However, only the prediction methods for the resistance and initial stiffness of bolted connection are provided in Eurocode 3, rather than the full load-deformation relationship of bolted connection, even though bolted angle could be treated as a special T-stub.
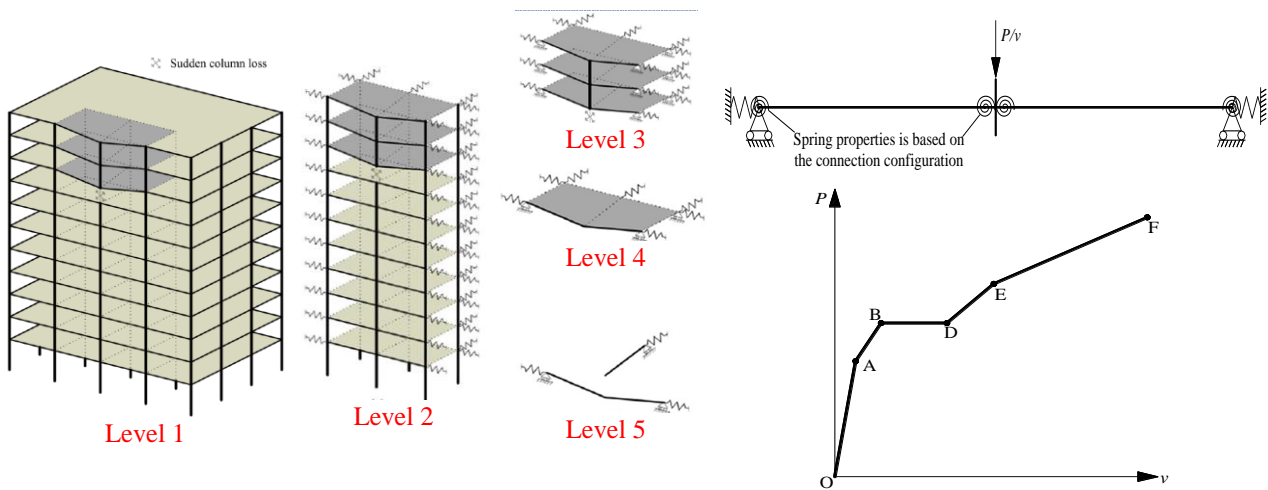
(a) Sub-structural levels for progressive collapse assessment [37]   (b) Performance of simplified sub-structure [38]

(c) Component-based properties prediction for the simplified spring of bolted angle connection
Fig. 2 Beam-column joint against progressive collapse

Yang [39] and Gong[40] both conducted tests and developed the mechanical models for the bolted angle connections under tension, aiming to predict the full vertical load-deformation relationship of the sub-structure against progressive collapse. However, their researches are still limited for only considering some key parameters. To achieve a better understanding of the mechanical performance of bolted angle connections under tensile load in the beam-column joint against progressive collapse as shown in Fig. 2, a test program of 20 bolted angle connections, was conducted in this study to investigate the mechanical behaviors of this type of connections. The key responses of the bolted angle connection such as the connection strength, deformation capacities and the influences of various connection parameters on the connection performance are evaluated. Based on the experimental results and the corresponding theoretical analysis, a mechanical model of bolted angle connection is proposed to predict its initial stiffness, ultimate bearing capacity and ultimate deformation and verified against the tested results and other mechanical models.

2. Experimental design

2.1. Specimen preparation

Fig. 3 shows the configuration of test connection. The dimensions of angle are $L_H{\times}L_V{\times}L_L{\times}t$ as summarized in Fig. 3 and Table 1. Total 20 specimens were divided into 10 groups (A0-A9), each group containing two parallel specimens with the same dimensions. Six parameters of bolted angle connection were investigated in the testing program: angle thickness t, bolt diameter d, horizontal bolt pitch g_H, vertical bolt pitch g_V, longitudinal bolt pitch g_L and bolt preload P. During the test, one of the parallel specimens was applied bolt preload, while the other one was not. The designation of bolted angle connection consists of three parts: group number, bolt preload and parameters variation. Taking the specimen A1-P-t8 and A1-NP-t8 as an example: A1 is the specimen group number; P and NP respectively represent whether or not bolt preload is applied; t8 means the angle thickness is 8mm.

All the used M20 and M24 bolts were Chinese Grade 8.8. The diameter of the bolt hole is about 2.0 mm larger than that of the bolts. The slip coefficient was 0.35 for the angle with paint according to Chinese standard JGJ82-2011 by where the preload applied on the 20-mm and 24-mm-diameter bolts were provided. The installation torque was derived by multiplying the preload, bolt diameter and torque-pretension coefficient which was 0.15. In order to prevent nut tripping due to quality problems, double nuts were used for tightening during the test.
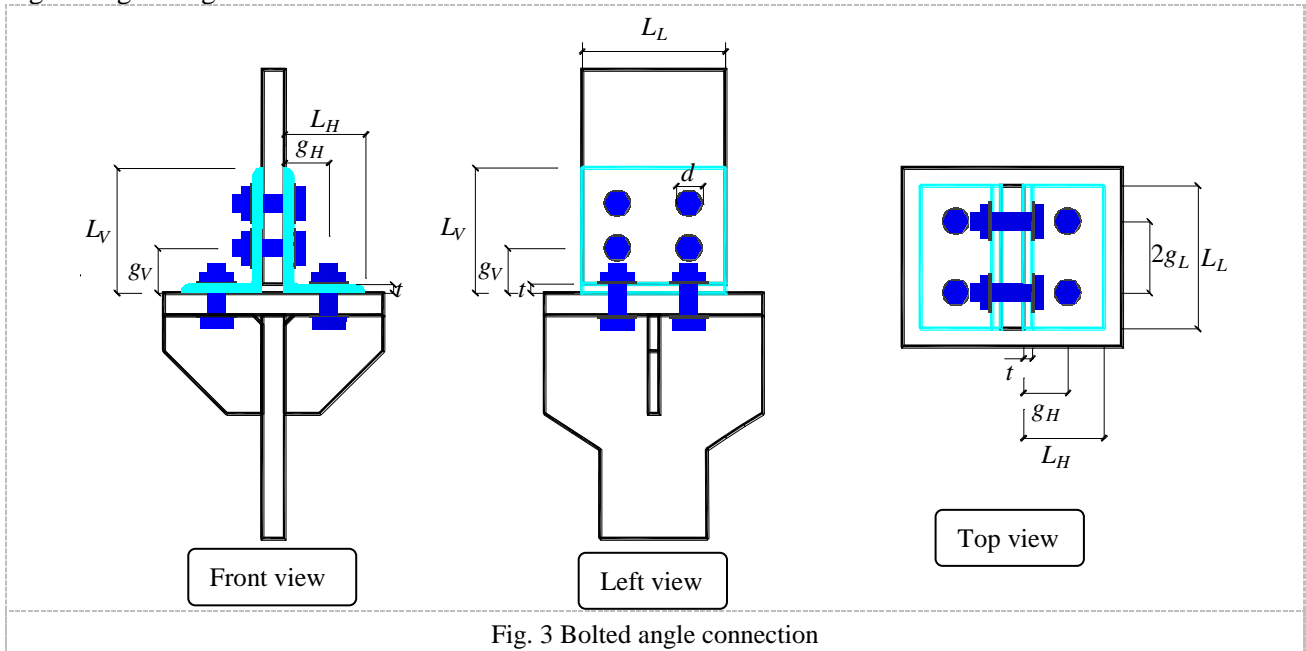
Fig. 3 Bolted angle connection

Table 1 Parameters of specimens

Specimen No.	L_V /mm	L_H /mm	L_L /mm	t /mm	g_H /mm	g_V /mm	g_L /mm	d /mm	Preload /kN
A0-P	140	90	160	10	50	50	40	20	125
A0-NP	140	90	160	10	50	50	40	20	0
A1-P-t8	140	90	160	**8**	50	50	40	20	125
A1-NP-t8	140	90	160	**8**	50	50	40	20	0
A2-P-t12	140	90	160	**12**	50	50	40	20	125
A2-NP-t12	140	90	160	**12**	50	50	40	20	0
A3-P-H70	140	**140**	160	10	**70**	50	40	20	125
A3-NP-H70	140	**140**	160	10	**70**	50	40	20	0
A4-P-H90	140	**140**	160	10	**90**	50	40	20	125
A4-NP-H90	140	**140**	160	10	**90**	50	40	20	0
A5-P-V70	**160**	100	160	10	50	**70**	40	20	125
A5-NP-V70	**160**	100	160	10	50	**70**	40	20	0
A6-P-V90	**160**	100	160	10	50	**90**	40	20	125
A6-NP-V90	**160**	100	160	10	50	**90**	40	20	0
A7-P-L50	140	90	**180**	10	50	50	**50**	20	125
A7-NP-L50	140	90	**180**	10	50	50	**50**	20	0

A8-P-L60	140	90	**200**	10	50	50	**60**	20	125
A8-NP-L60	140	90	**200**	10	50	50	**60**	20	0
A9-P-d24	140	90	160	10	50	50	40	**24**	175
A9-NP-d24	140	90	160	10	50	50	40	**24**	0

Note: L_V is the length of vertical leg of angle; L_H is the length of horizontal leg of angle; L_L is the length of angle g_H is the length of horizontal bolt pitch; g_v is the length of vertical bolt pitch; g_L is the length of longitudinal bolt pitch; t is the angle thickness; d is the bolt diameter

Angles and loading devices were all made of Chinese Q235 grade steel. Tensile coupons were cut from the angles. The elastic modulus E_s, yield strength f_y and ultimate strength f_u and the ultimate strain ε_u according to the ultimate strength of the steel were tested and summarized in Table 2. The mechanical properties of the bolts were provided by the suppliers.

Table 2 Material property of the specimens

Specimens	Thickness(diameter)/mm	f_y/MPa	f_u/MPa	E_s/MPa	ε_u
Angle	8	208	400	1.97×10^5	0.33
	10	209	410	2.02×10^5	0.34
	12	194	402	2.03×10^5	0.33
M20	20	628	811	2.34×10^5	0.09
M24	24	633	864	2.34×10^5	0.09

2.2. Test procedure

The specimens were tested on MTS universal testing machine, as shown in Fig. 4. Each specimen consists of a pair of angles and eight connecting bolts. The horizontal leg of angle was installed on the loading device by tensile bolts. The vertical leg of angle was connected to the upper loading plate by shear bolts. Upper and lower loading plate were clamped by the top and bottom clamping heads respectively. The loading was controlled by displacement loading method at 0.025 mm/s until the specimen failed due to bolt or angle fracture.
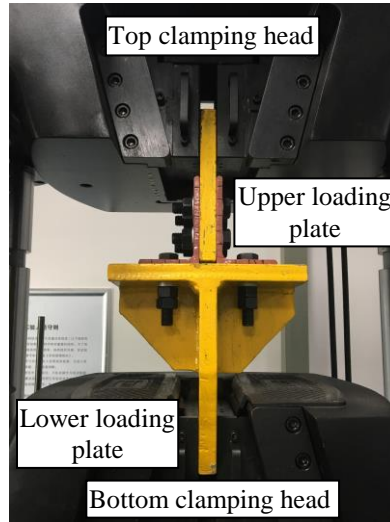

Fig. 4 Testing machine

2.3. Experimental results

2.3.1 Deformation process

The deformation process of the specimen under the action of pure tension is divided into four stages: (1) elastic stage; (2) plastic stage; (3) transitional stage; (4) bolted angle connections plastic deformation stage. In addition, to consider the bolt slip stage, Yang [39] divided the deformation process into five stages. Gong [40] divides the displacement curve into three stages on the basis of the Eurocode Component Method. Since no obvious bolt slip was observed in the experiment, the bolt slip stage was not considered separately and was included in the elastic stage. Taking the standard specimens as an example, the load-displacement curve of A0-P and A0-NP is given in Fig. 5.

In the stage 0-A/0-A*, the load applied by the testing machine is resisted primarily by the friction of the vertical loading plate resulting from the bolt preload. After the tension of the testing machine reaches the slip friction strength of the bolt, it begins to slip. Until bolt shanks contact with the holes, deformation into the stage A-B/A*-B*, the load is transmitted to angle by the contact between holes and bolt shanks and. Due to the preload is diminished, section B-C/B*-C* shows a slightly lower stiffness than seciton A-B/A*-B*. Then, the

4

load-displacement curve enters the plastic deformation stage of connections C-D/C*-D*, with geometric nonlinearity and material hardening [39] formed in bolt shanks and angle.
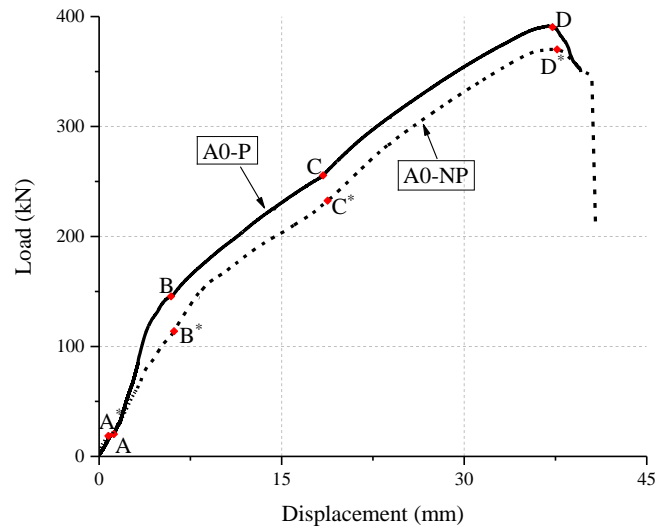

Fig. 5 Load-displacement carve of A0-P and A0-NP

2.3.2 Failure modes

Table 3 and Figs. 6-10 summarize five failure modes of the 20 bolted angle connections observed in the tests. The failure mode of angle fracture at heel was observed in most specimens, as indicated in Fig. 6. The failure mode of angle fracture at bolt holes line and bolt fracture with yielded angle was observed in A1 and A2 group, respectively, as shown in Fig. 7 and Fig. 8. Angle fracture at bolt holes line with yielded bolt was observed in A3 and A4 group, as indicated in Fig. 9. The failure mode, namely angle fracture close to heel, was observed in A5 and A6 group, as shown in Fig. 10.

Three kinds of angle thickness of 8mm, 10mm and 12mm were used in the test, the failure modes of the connections were angle fracture at bolt holes line, angle fracture at heel and bolt fracture with yielded angle respectively. This may be due to the difference in stiffness ratio between bolts and angle. In other words, the matching between the dimensions of bolt and angle also affects the deformation capacity of bolted angle connection.

When the horizontal bolt pitch g_H increased from 50mm to 90mm, the failure modes varied from angle fracture at heel to angle fracture at bolt holes line with yielded bolt. Correspondingly, when the vertical bolt pitch g_V increased from 50mm to 90mm, the failure modes changed from angle fracture at heel to angle fracture close to heel. While, the varies of longitudinal bolt pitch g_L, bolt diameter d and bolt preload P were did not changes the failure mode of the connections.
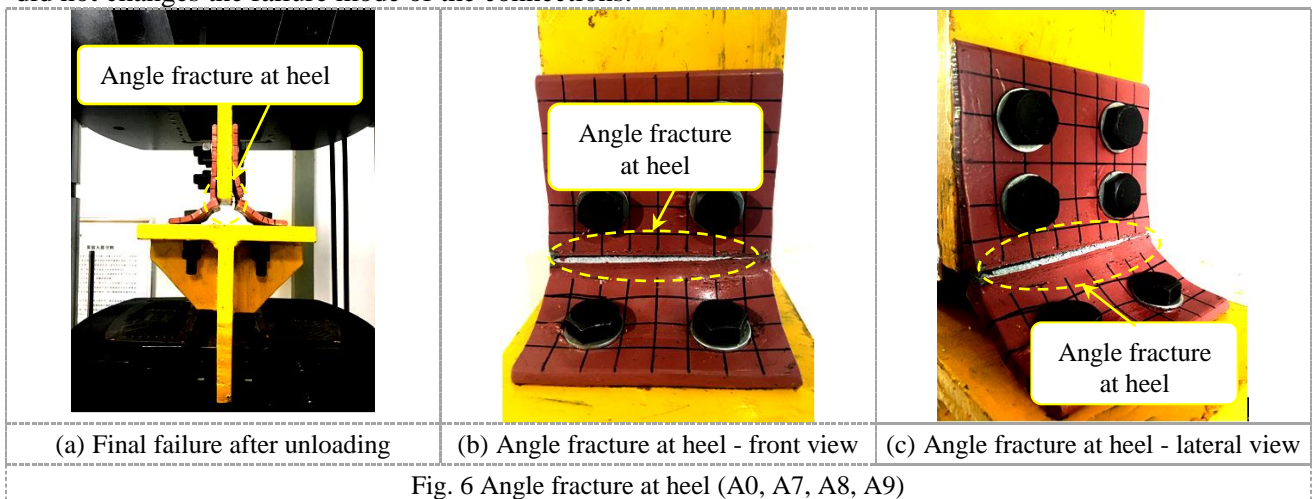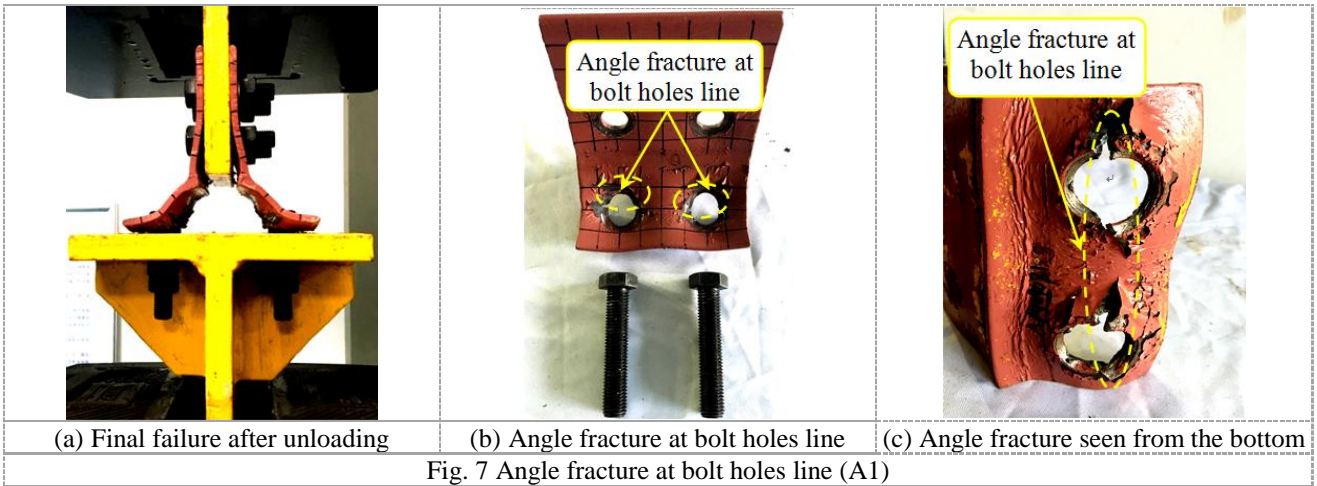
| (a) Final failure after unloading | (b) Angle fracture at heel - front view | (c) Angle fracture at heel - lateral view |

Fig. 6 Angle fracture at heel (A0, A7, A8, A9)

| (a) Final failure after unloading | (b) Angle fracture at bolt holes line | (c) Angle fracture seen from the bottom |

Fig. 7 Angle fracture at bolt holes line (A1)

| (a) Final failure after unloading | (b) Angle yielded under tension | (c) Bolt fracture |

Fig. 8 Bolt fracture with yielded angle (A2)

| (a) Final failure after unloading | (b) Angle fracture at bolt holes line | (c) Bolt yielded under tension |

Fig. 9 Angle fracture at bolt holes line with yielded bolt (A3, A4)

| (a) Final failure after unloading | (b) Angle fracture close to heel | (c) Angle fracture under tension |
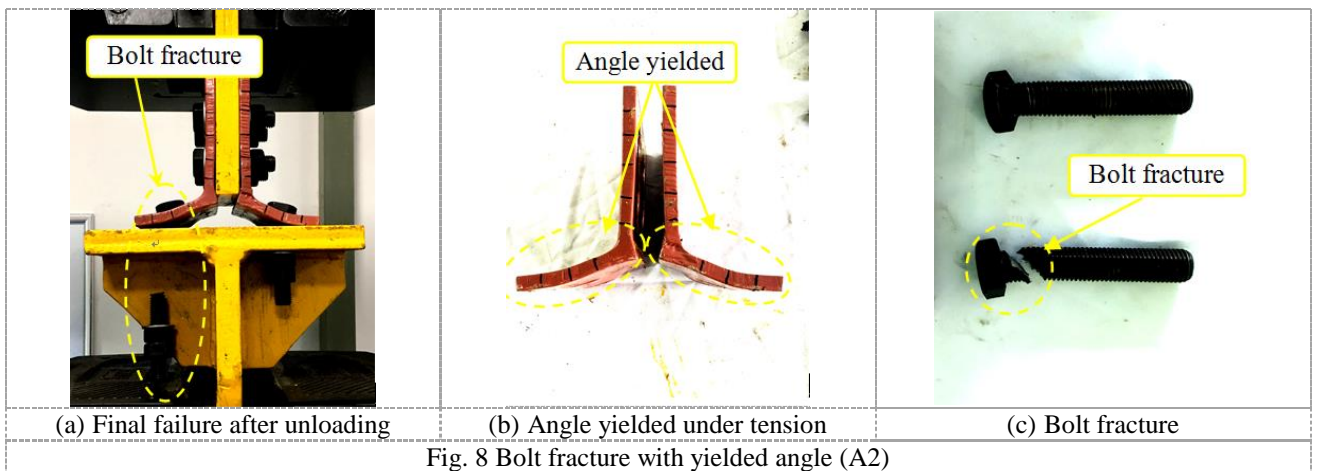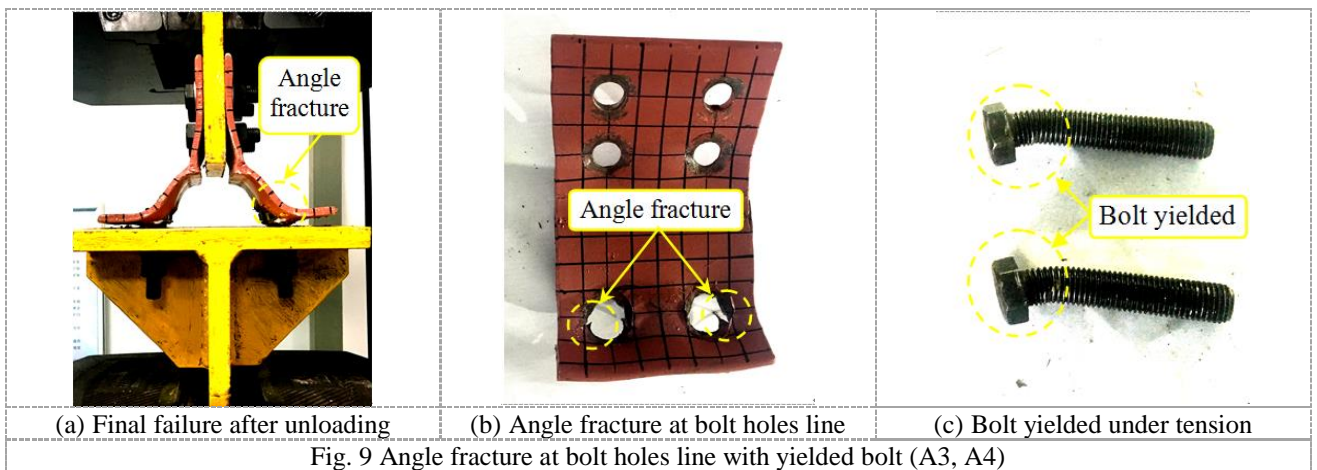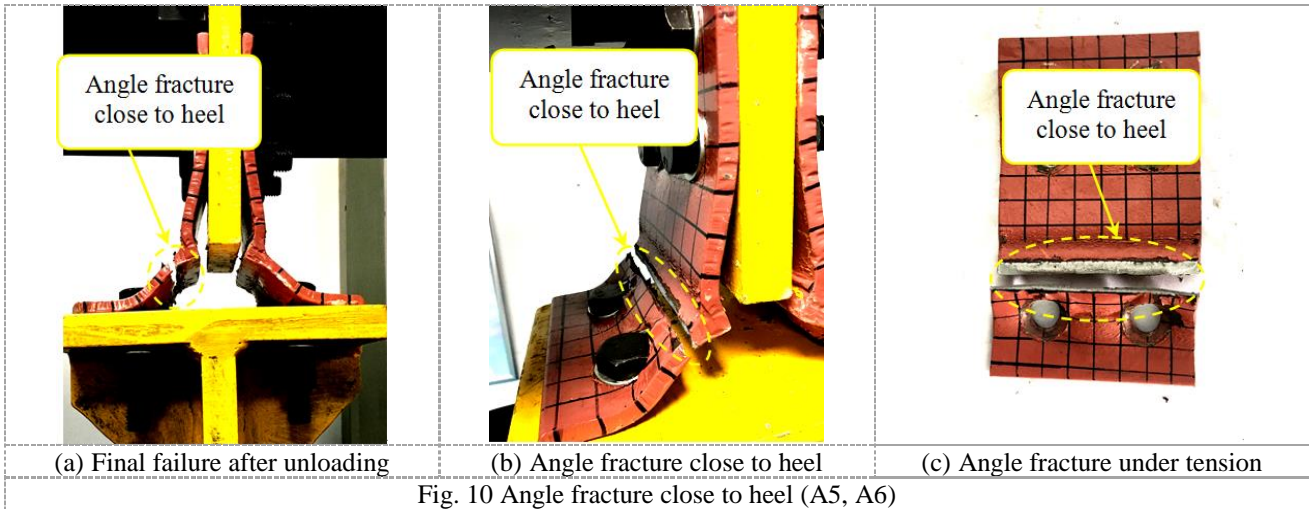
Fig. 10 Angle fracture close to heel (A5, A6)

		Table 3 Failure modes		
Specimen No.	Ultimate load /kN	Ultimate displacement /mm	Initial stiffness /(kN/mm)	Failure mode
A0-P	391	37	38	Angle fracture at heel
A0-NP	370	37	20	Angle fracture at heel
A1-P-t8	359	46	35	Angle fracture at bolt holes line
A1-NP-t8	362	48	19	Angle fracture at bolt holes line
A2-P-t12	468	30	33	Bolt fracture with yielded angle
A2-NP-t12	481	31	23	Bolt fracture with yielded angle
A3-P-H70	417	69	14	Angle fracture at bolt holes line with yielded bolt
A3-NP-H70	438	76	11	Angle fracture at bolt holes line with yielded bolt
A4-P-H90	426	78	11	Angle fracture at bolt holes line with yielded bolt
A4-NP-H90	438	80	9	Angle fracture at bolt holes line with yielded bolt
A5-P-V70	411	44	22	Angle fracture close to heel
A5-NP-V70	430	42	21	Angle fracture close to heel
A6-P-V90	436	51	19	Angle fracture close to heel
A6-NP-V90	336	51	17	Angle fracture close to heel
A7-P-L50	449	48	39	Angle fracture at heel
A7-NP-L50	391	39	21	Angle fracture at heel
A8-P-L60	458	51	41	Angle fracture at heel
A8-NP-L60	449	47	24	Angle fracture at heel
A9-P-d24	409	37	32	Angle fracture at heel
A9-NP-d24	380	31	28	Angle fracture at heel

2.3.3 Load-displacement curves

The investigated parameters in the experiments include angle thickness t, horizontal bolt pitch g_H, vertical bolt pitch g_V, longitudinal bolt pitch g_L, bolt diameter d and bolt preload P.

(1) Effect of angle thickness

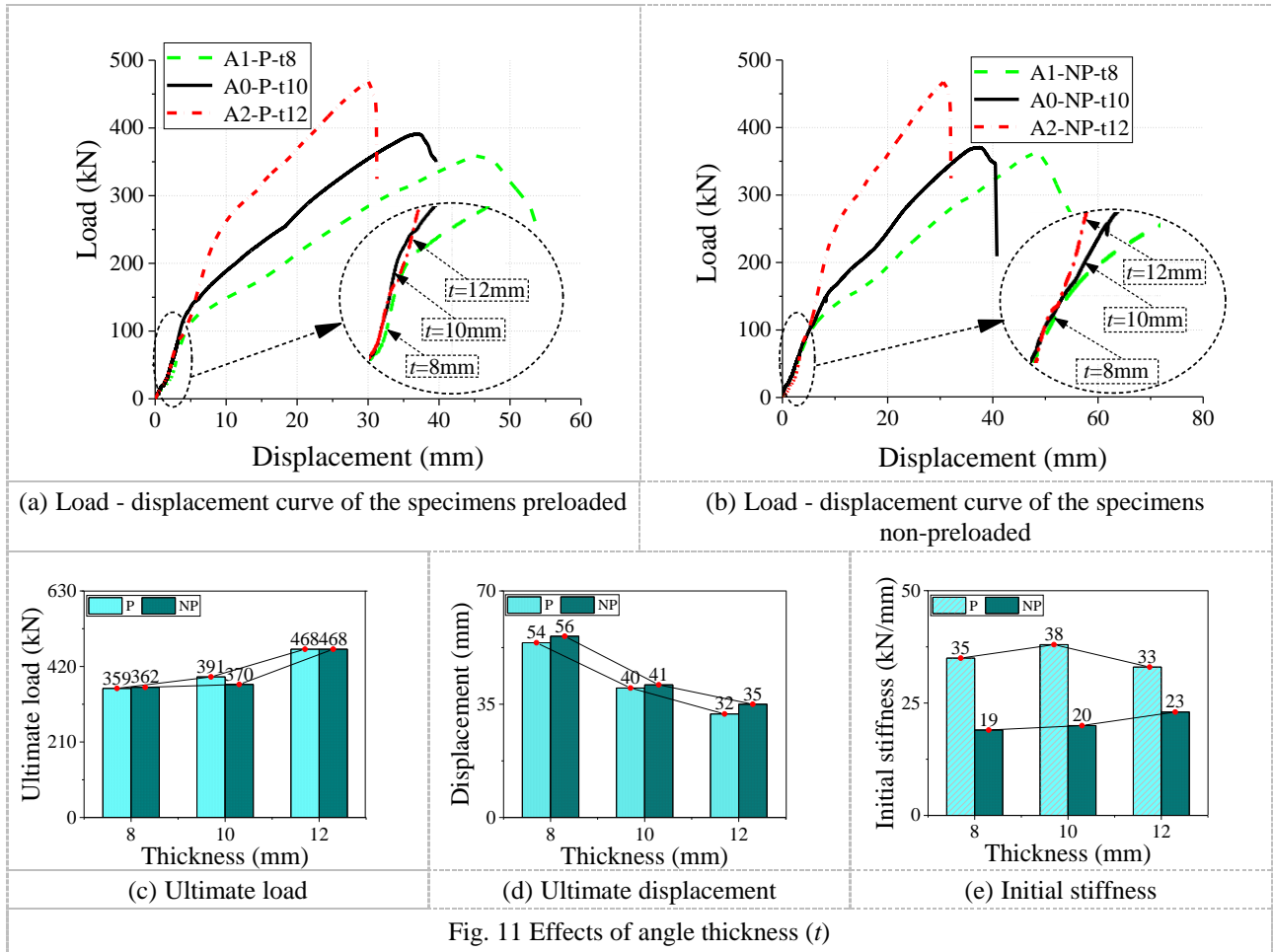When the angle thickness increases from 8mm to 12mm, the bearing capacity, stiffness and deformation capacity of the connection all vary, as shown in Fig. 11. It can be observed from the load-displacement curve that the yield point of the connection does not change significantly with the increase of angle thickness. The angle thickness also shows no significant influence on the deformation stiffness of the connection, while the ultimate bearing capacity and ultimate deformation of the connection are positively and negatively correlated with the angle thickness respectively, as shown in Fig. 11(c and d). Piluso et al. [41] proposed that increasing end plate thickness would reduce the deformation capacity of the connection which was verified in the experiment. The initial stiffness of the connections is mainly affected by the bolt preload. At the same time, with the increase of angle thickness, the initial stiffness of the connection also increases gradually, as indicated in Fig. 11(e). The initial stiffness of specimen A2-P-t12 seems lower than that of A0-P-t10, probably due to data acquisition errors during the experiment.
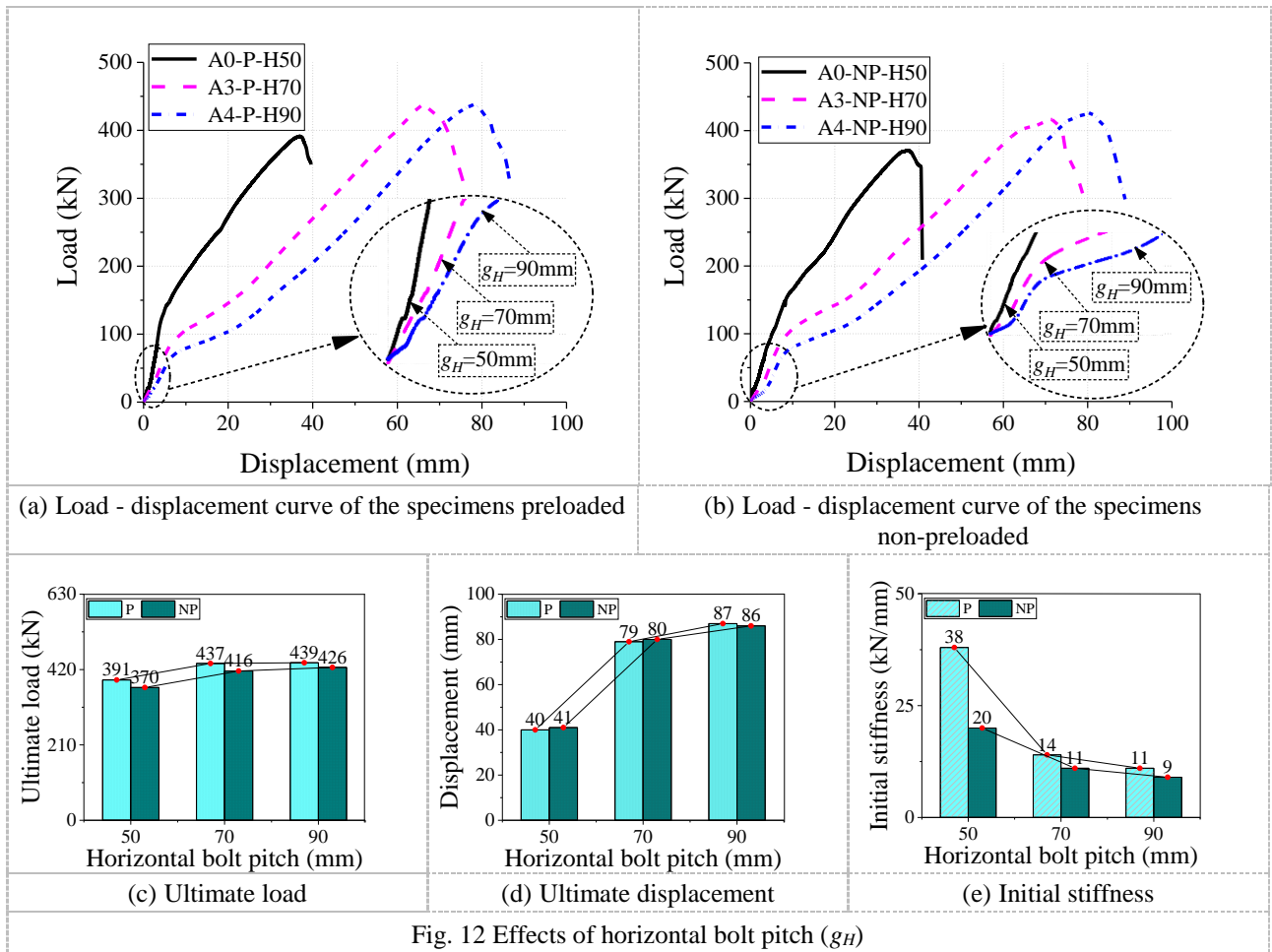
7

(a) Load - displacement curve of the specimens preloaded

(b) Load - displacement curve of the specimens non-preloaded

(c) Ultimate load

(d) Ultimate displacement

(e) Initial stiffness

Fig. 11 Effects of angle thickness (t)

(2) Effect of horizontal bolt pitch

Three horizontal bolt pitch g_H (50mm, 70mm, and 90mm) were designed in the test. When the horizontal bolt pitch g_H increases from 50mm to 90mm, the failure mode of the connection changes from angle fracture at heel to angle fracture at bolt holes line with yielded bolt. The fracture position of angle changes, which may be due to the increase of the horizontal bolt pitch g_H. The increase of the horizontal bolt pitch g_H increases the deformation capacity of the connection, which leads to the fracture position is transferred from the heel to the center line of bolt holes.

From the load-displacement curve, as shown in Fig. 12(a and b), when g_H is 70mm and 90mm, the curve shape of the connection is significantly different from that when g_H is 50mm. When g_H is 70mm and 90mm, the load-displacement curve not only rises slowly in the elastic section, but also presents an obvious transition section, which fully reflects the deformation process of horizontal leg of angle. This is quite different from the load-displacement curve when g_H is 50mm. The increase of horizontal bolt pitch g_H decreases the deformation stiffness of the connection, as shown in Fig. 12(a and b). The initial stiffness of the connection is also negatively correlated with the horizontal bolt pitch g_H, as shown in Fig. 12(e).

The ultimate bearing capacity of the connection increases with the increase of the horizontal bolt pitch g_H whether or not the bolt preload is applied, as shown in Fig. 12(c). This is different from Yang [39]. The reason for the difference may result from the dimension of the angle. When g_H is 50mm, the dimension of angle is L140×90×10mm, while when g_H is 70mm and 90mm, the dimension of angle is L140×140×10mm.

In terms of ductility, the increase of the horizontal bolt pitch g_H enhances the deformation capacity of the connection, as shown in Fig. 12(e). In addition, when g_H increases from 50mm to 70mm, the ultimate deformation of the connection is approximately doubled. It can be seen that when the horizontal bolt pitch g_H increases to a certain degree, the ultimate deformation of the bolted angle connection shows little change.

8

(a) Load - displacement curve of the specimens preloaded

(b) Load - displacement curve of the specimens non-preloaded

(c) Ultimate load

(d) Ultimate displacement

(e) Initial stiffness

Fig. 12 Effects of horizontal bolt pitch (g_H)

(3) Effect of vertical bolt pitch

As expected, the vertical bolt pitch g_V has direct effect on the performance of the connections, which refers to the failure mode and the curves referring to different vertical bolt pitch g_V. When the vertical bolt pitch g_V increases from 50mm to 90mm, the fracture position of angle is changed from "at heel" to "close to heel". By increasing the length of g_V, the distance between bolt holes line on angle vertical leg and angle horizontal leg is increased, thus improving the deformation capacity of angle vertical leg. From the load-displacement curves, when the g_V is 50mm, 70mm and 90mm respectively, the three curves are roughly in the same shape, as shown in Fig. 13(a and b). The vertical bolt pitch g_V affects the ultimate load, initial stiffness and ultimate deformation of the connection. Fig. 13(c) shows that with the increase of g_V, the ultimate bearing capacity of the connection gradually increases. With the same variation tendency of bearing capacity, the ultimate deformation of the connection also increases with the increase of g_V, as indicated in Fig. 13(d). However, the initial stiffness of the connection gradually decreases with the increase of g_V, as shown in Fig. 13(e). It can be concluded that the influence of g_V on the deformation capacity of connection is not as significant as that of g_H.
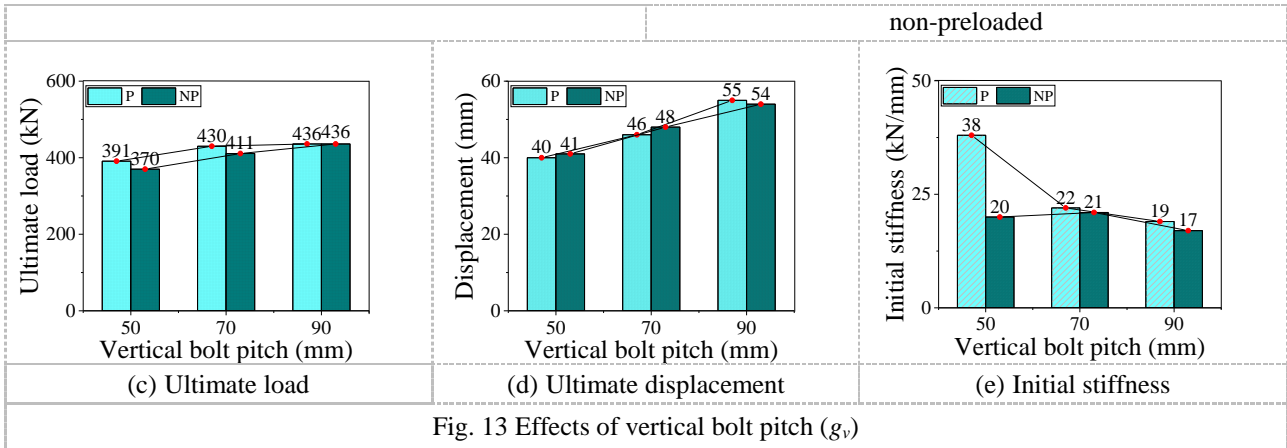

(a) Load - displacement curve of the specimens preloaded

(b) Load - displacement curve of the specimens

(c) Ultimate load

(d) Ultimate displacement

(e) Initial stiffness
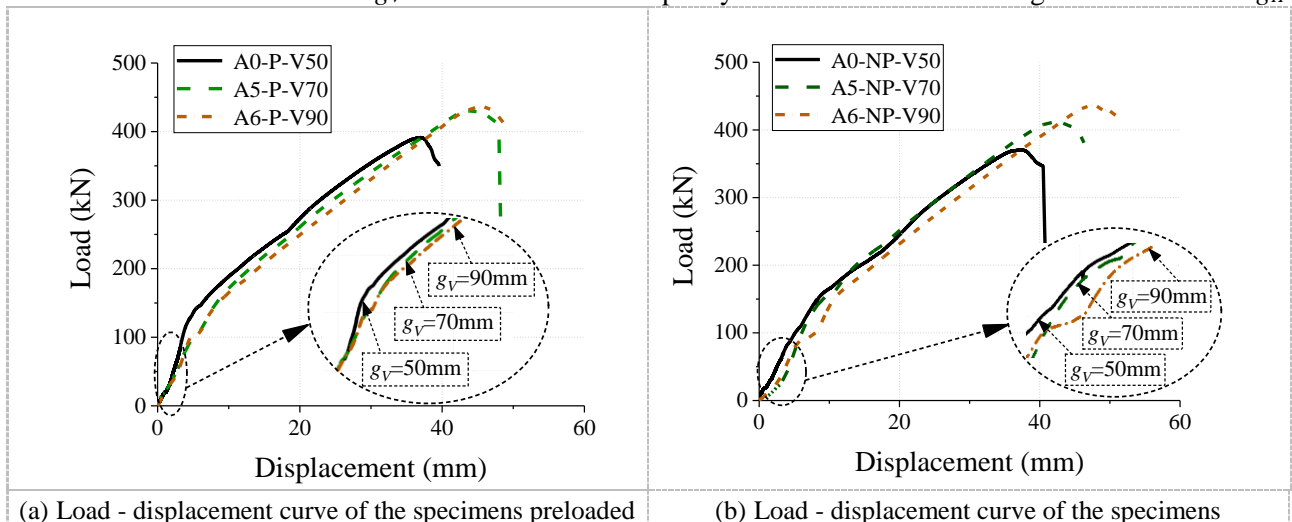
Fig. 13 Effects of vertical bolt pitch (g_v)

(4) Effect of longitudinal bolt pitch

Three longitudinal bolt pitch g_L are considered in the experiment, namely 40mm, 50mm and 60mm. Varying g_L does not change the failure modes of the connections, namely all the angle fractured at heel. From the load-displacement curves, the increase of g_L changes the mechanical properties of the connection, as shown in Fig. 14(a and b). With the increase of g_L, the peak point of the curve varies gradually. The change of g_L has little effect on the yielded point and deformation stiffness of connections. Due to the same failure mode, the trend and shape of the curve are basically the same when g_L is 40mm, 50mm and 60mm respectively.

As shown in Fig. 14(c and d), compared with the standard specimen A0-NP-L40, the bearing capacity of specimens A7-NP-L50 and A8-NP-L60 are increased by 5.8% and 21.4% respectively and the deformation capacity increased by 4.7% and 22.3% respectively. Compared with A0-P-L40, the bearing capacity of A7-P-L50 and A8-P-L60 are increased by 14.8% and 17.1% and the ultimate deformation capacity increased by 30.1% and 45.2%. Longitudinal bolt pitch g_L has little effect on the initial stiffness, which is mainly affected by the bolt preload, as indicated in Fig. 14(e).

(a) Load - displacement curve of the specimens preloaded

(b) Load - displacement curve of the specimens non-preloaded

(c) Ultimate load

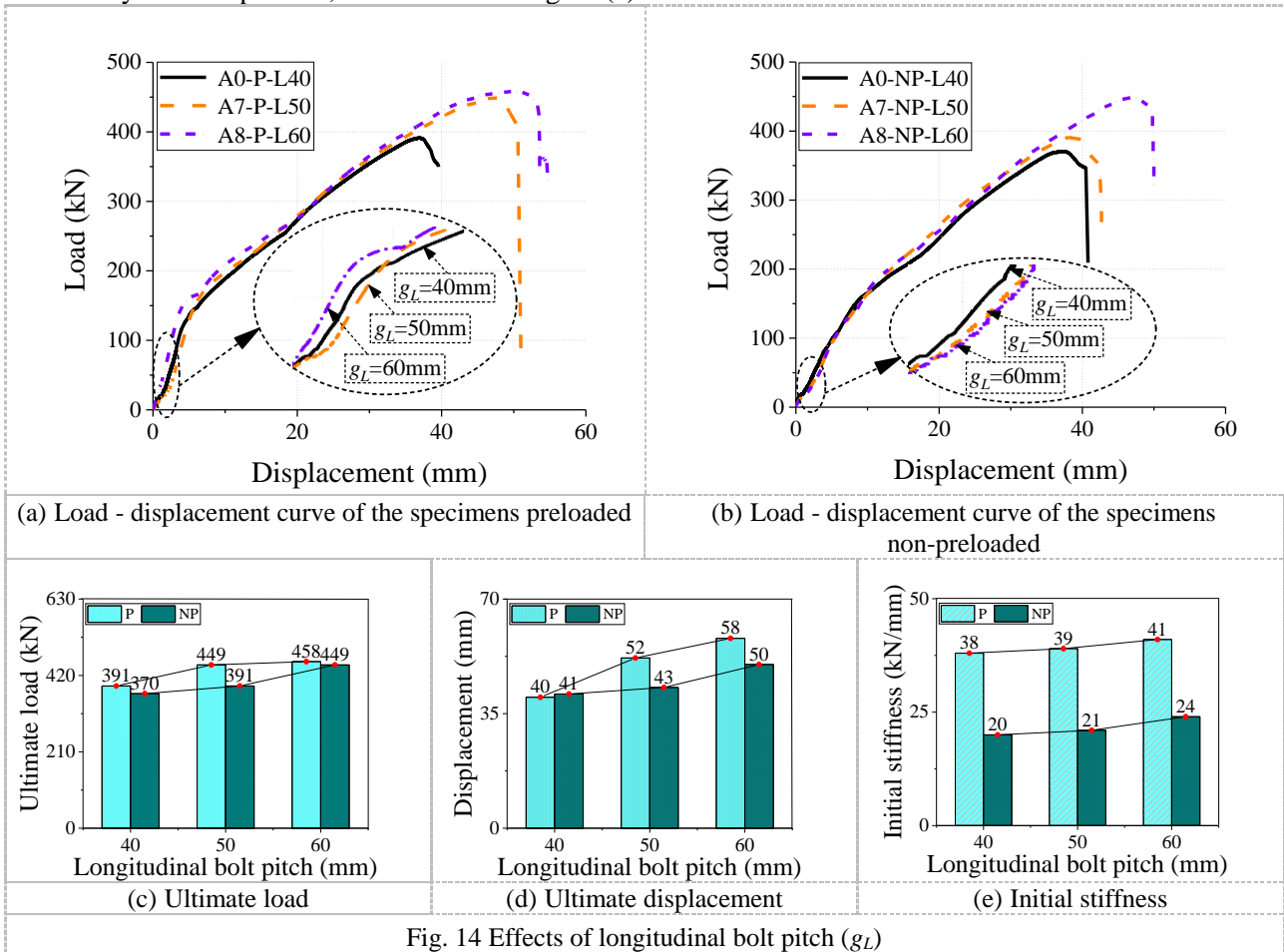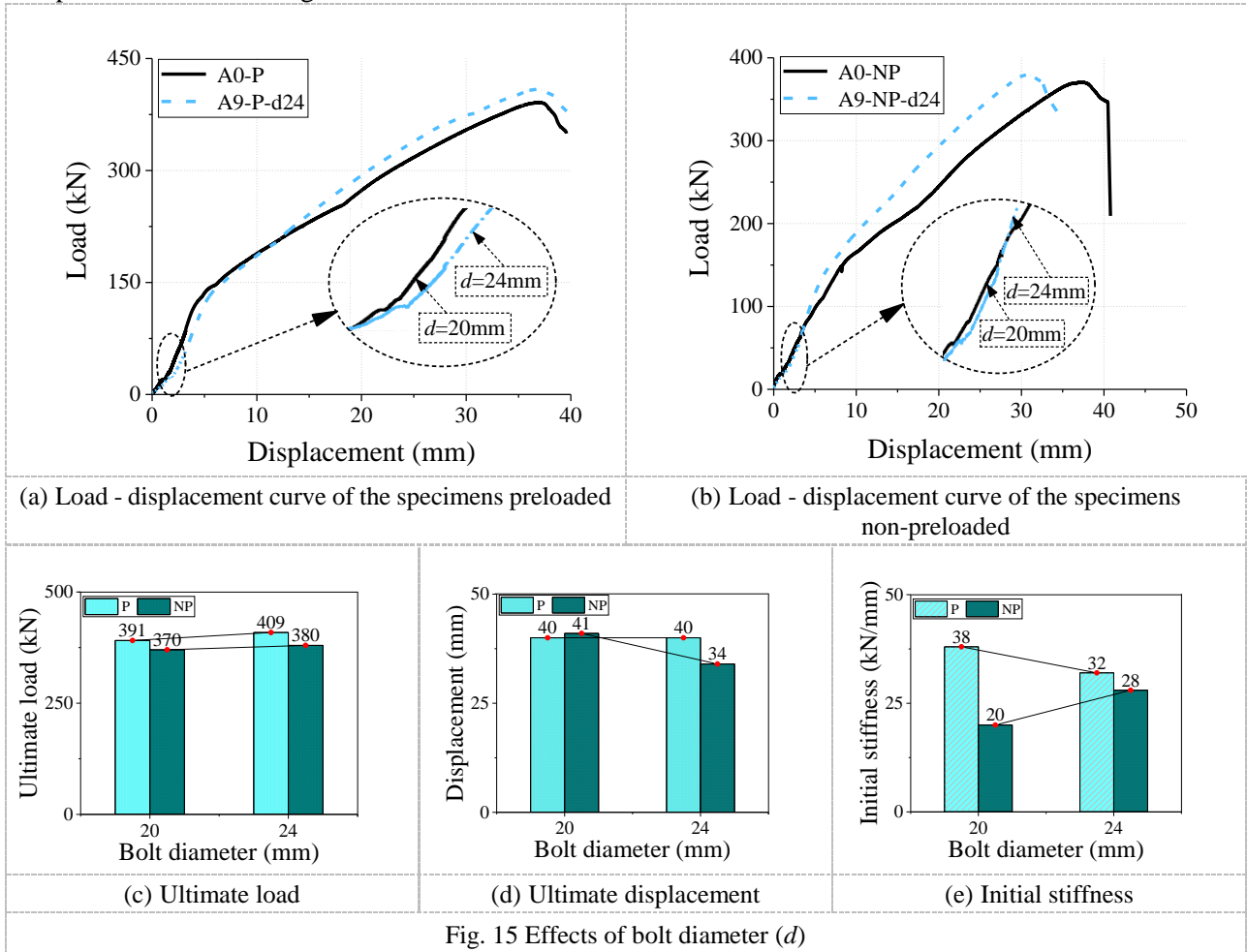(d) Ultimate displacement

(e) Initial stiffness

Fig. 14 Effects of longitudinal bolt pitch (g_L)

(5) Effect of bolt diameter

10

M20 and M24 bolt diameters were considered in the experiment. Fig. 15(a and b) shows the load-displacement curves of specimens A0-P, A9-P-d24, A0-NP and A9-NP-d24. As can be seen from the figures, increasing the bolt would increase the stiffness of the connection slightly. Compared with the standard specimens A0-P and A0-NP, the ultimate bearing capacity of A9-P-d24 is increased by 17.6kN and 9.3kN for A9-NP-d24. As the bolt diameter increases, the ultimate bearing capacity of the bolted angle connection increases slightly, as shown in Fig. 15(c). Fig. 15(d) analyzes the deformation capacity of connections under different bolt diameters. It is observed from the experimental results that the deformation capacity of connections decreases by increasing bolt diameter. This may result from the fact that the increase in bolt hole and screw head diameters would reduce the real value of horizontal gauge length g_H and result in a smaller deformation capacity of bolted angle connections. As can be seen in Fig. 15(e), the initial stiffness of the specimen A9-P-d24 is smaller than that of the specimen A0-P-d20, which may be due to the relaxation of the bolt preload before loading.

(a) Load - displacement curve of the specimens preloaded

(b) Load - displacement curve of the specimens non-preloaded

(c) Ultimate load

(d) Ultimate displacement

(e) Initial stiffness

Fig. 15 Effects of bolt diameter (*d*)

(6) Effect of bolt preload

Fig. 16 compares the load-displacement curves of the two specimens with and without bolt preload under the same dimensions. The experimental results show that the initial stiffness of the bolted angle connection with bolt preload is greater than that of the connections without bolt preload. From the curve shape, the yield point of the joint is higher than that of the specimen without bolt preload. However, the bolt preload does not affect the ultimate deformation of bolted angle connection. Applying bolt preload does not affect the failure mode of the connection. The coincidence in two curves in Fig. 16 (j) may also result from the relaxation of the bolt preload before loading.
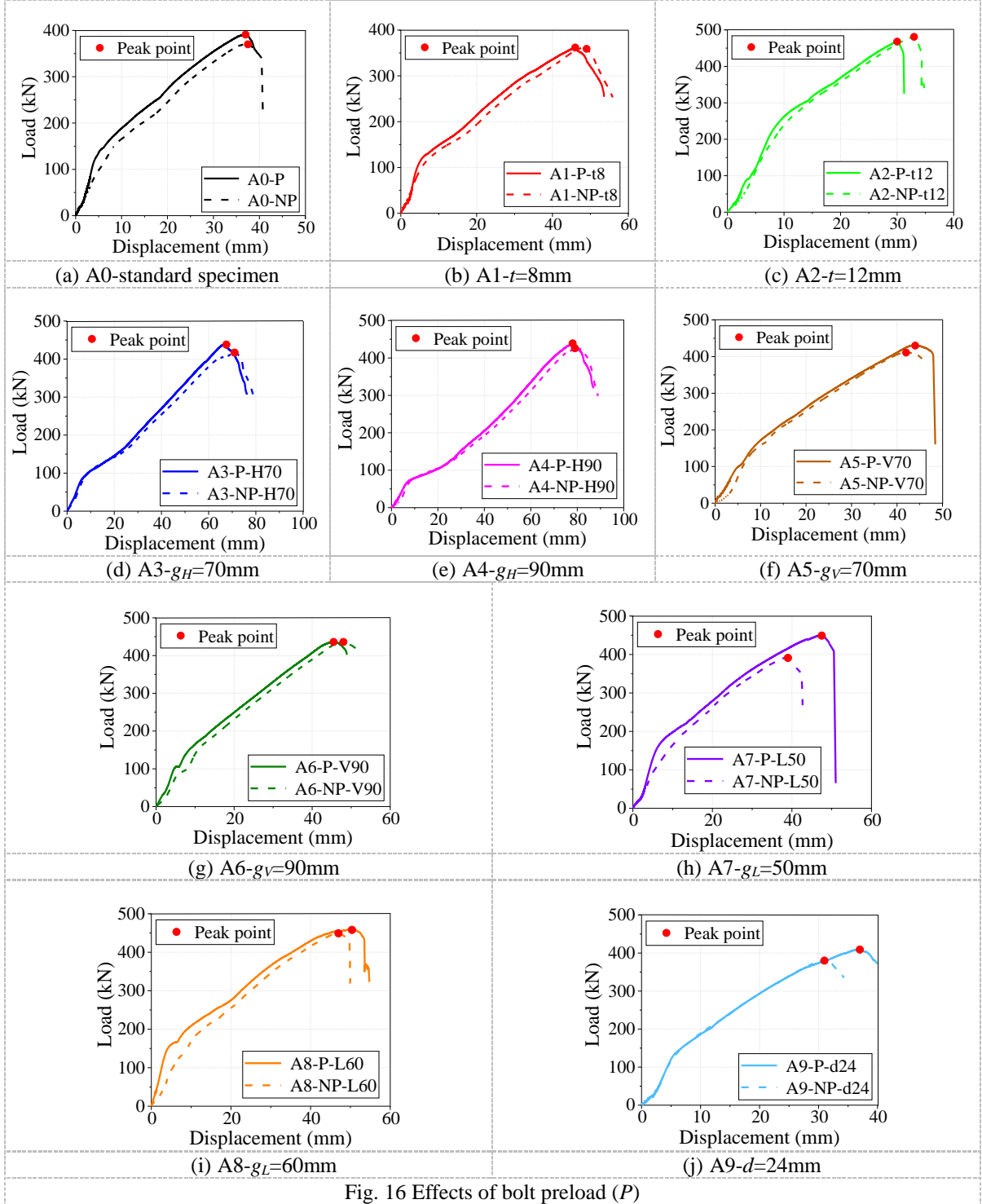
Fig. 16 Effects of bolt preload (P)

3. Mechanical performance of bolted angle connections

3.1. Deformation capacity

The deformation capacity of bolted angle connection is affected by both bolt and angle. Under the action of monotonic tensile, firstly, bending deformation occurs on the horizontal leg. Then, the deformation subsequently extends to the vertical leg. As the tensile load increases, the screw and angle contact with each other and the screw shows bending deformation to a certain extent. The fracture of angles or bolts determines the deformation capacity of the connection.

BCSA/SCI [42] provided Eq. (1) for the deformation capacity $\Delta_{u\text{-}SCI}$ of bolted angle connections

$$\Delta_{u-SCI} = 2.6 \frac{L_H}{t} \frac{g_H}{60} \leq 30mm \tag{1}$$

where L_H is the length of angle horizontal leg, g_H is the horizontal bolt pitch and t is the angle thickness.

12

Eq. (1) shows that the length of angle horizontal leg L_H affects the ultimate deformation of the connection. By observing the deformation of angle from the test results, it is found that no significant deformation occurs along the bolt holes line to the free end of the angle horizontal leg, as show in Fig. 17. This phenomenon is consistent with the conclusion drawn by Yang [39].

In addition, only three parameters are considered in Eq. (1). However, it can be seen from the experimental results, besides the factors taken into account in the formula, many other parameters which have not been covered in this model, such as bolt diameter, vertical bolt pitch and longitudinal bolt pitch, also have an effect on the deformation capacity of the bolted angle connections.

By considering the failure modes of the connections, Shen and Astaneh-Asl [23-24] developed the formulas applicable to angle fracture or bolt fracture respectively.

$$\Delta_{u-Sh} = 2(g_H - t)\varepsilon_u \sqrt{t/(g_H - t)\varepsilon_u} \quad \text{for angle fracture} \tag{2}$$

$$\Delta_{u-Sh} = \frac{L_H + g_H}{2} \tan(\varepsilon_u) \qquad \text{for bolt fracture with yielded angles} \tag{3}$$

where ε_u is the ultimate strain.

Different from BCSA/SCI, these formulas proposed by Shen and Astaneh-Asl considered the material properties of angle.

Yang [39] proposed the following formula with regard to the interaction between angles and bolts where horizontal bolt pitch g_H was substituted with g_H^*

$$\Delta_{u-Y} = g_H^*(1+\varepsilon_u)\sin(\frac{\varepsilon_u g_H^*}{2t}) \tag{4}$$

$$g_H^* = g_H - t - 0.8r_a + \eta d_b \tag{5}$$

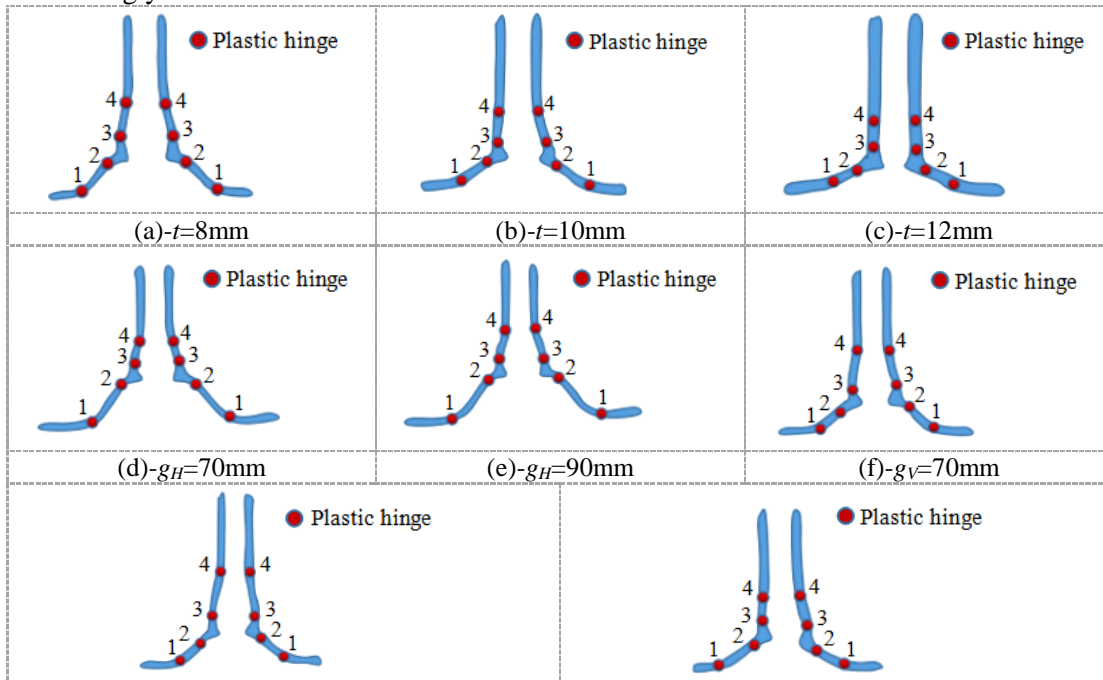where g_H^* represent the distance between the two plastic hinges at the horizontal legs of angles.

$$\eta = 1.1335 - 0.00242\frac{F_b}{F_g} \tag{6}$$

where η is a factor regarding the ratio between the axial resistance of bolts F_b ($F_b = f_{y,b}A_b$) and the yield strength of angle legs F_g ($F_g = F_{T,Rd}/b_{eff,a}$) [39].

Through a regression analysis, a new formula for estimating the ultimate deformation capacity of bolted angle connections was proposed by Gong [40]

$$\Delta_{u-G} = 11.4\sqrt{g_H/t} \tag{7}$$

In the aforementioned formulas for calculating the ultimate deformation of bolted angle connection, only the deformation of angle horizontal leg is considered. By observing the deformation of the angle in the test results, the deformation of the vertical leg of angle also contributes to the total deformation capacity of the connection. The angle deformation is shown in Fig. 17. When the horizontal leg is pulled up, the vertical leg deforms accordingly.

(a)-t=8mm (b)-t=10mm (c)-t=12mm

(d)-g_H=70mm (e)-g_H=90mm (f)-g_V=70mm

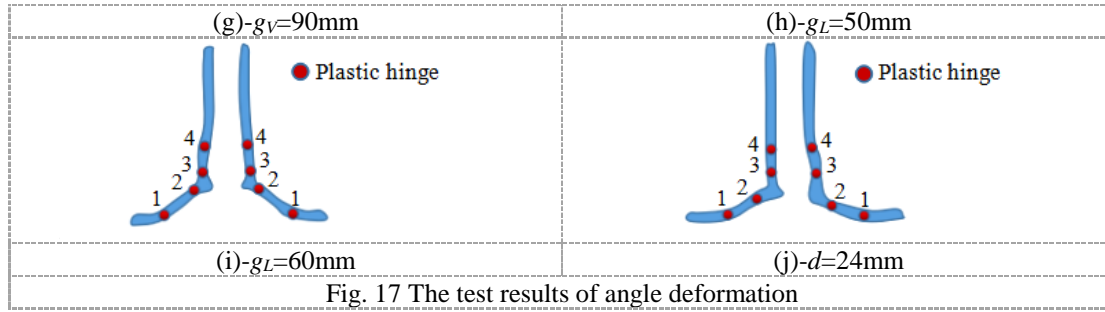| (g)-g_V=90mm	(h)-g_L=50mm
(i)-g_L=60mm	(j)-d=24mm

Fig. 17 The test results of angle deformation

It can be seen from Fig. 17 that the ultimate deformation shapes of angle under different parameters are different. Fig. 17(b) is the control specimen. The other parameters of this connection are t=10mm, g_H=50mm, g_V=50mm, g_L=40mm, and d=20mm.

Fig. 17(a-c) shows the ultimate deformation of the connections with different angle thicknesses. The thinner the angle is, the larger the horizontal leg and vertical leg of angle deform. Compared with Fig. 17(d and e), when g_H increases from 70mm to 90mm, the ultimate deformation shape of angle does not differ much. But compared with the standard specimen, the ultimate deformation shape of angle changes obviously. The influence of g_V and g_L on the ultimate deformation of angle is not as significant as g_H, as shown in Fig. 17(f and i). As indicated in Fig. 17(j), when the bolt diameter is increased, the deformation of the horizontal leg being pulled is significantly decreased and the deformation of the vertical leg is not as obvious as that when d=20mm.

Based on the experimental results and Yang's model [39], a formula for calculating the ultimate deformation of the bolted angle connection is developed in this paper by considering the deformation of the vertical leg:

$$\Delta u = \sqrt{g_H^{*2} + g_V^{*2}}(1+\varepsilon_u)\sin\theta \qquad (8)$$

$$g_V^* = g_V - t - 0.8r_a + \eta d_b \qquad (9)$$

where θ is measured at the angle at which the horizontal leg is being pulled up; ε_u is the ultimate strain; t is the angle thickness; r_a is the radius of the angle fillet; d_b is the bolt diameter; g_H^* and η are seen in Eq. (5-6) [39].

The deformation capacity predicted by the models from BCSA/SCI [42], Shen and Astaneh-Asl [23-24], Yang [39], Gong [40] and the proposed model, are compared in Table 4. For Specimen A9-NP-d24, the proposal model provides the most unconservative value (1.20). The most conservative prediction is found (0.92) for Specimen A1-NP-t8. The proposed model shows better accuracy than other models, even though a slight overestimation of the ultimate deformation is found. It should be mentioned that more tested data are needed to validate the proposed model and Yang's model [39], since some factors are derived directly from test.

Table 4 Analysis of ultimate displacement

Specimen	Test	Proposed model		BSCA/SCI		Shen and Astaneh-Asl		Yang's model		Gong's model	
	Δ_u /mm	$\Delta_{u\text{-}P}$ /mm	$\Delta_{u\text{-}P}/\Delta_u$	$\Delta_{u\text{-}SCI}$ /mm	$\Delta_{u\text{-}SCI}/\Delta_u$	$\Delta_{u\text{-}Shen}$ /mm	$\Delta_{u\text{-}Shen}/\Delta_u$	$\Delta_{u\text{-}YT}$ /mm	$\Delta_{u\text{-}YT}/\Delta_u$	$\Delta_{u\text{-}G}$ /mm	$\Delta_{u\text{-}G}/\Delta_u$
A0-P	37	40.2	1.04	19.5	**0.53**	23.4	**0.63**	44.0	**1.20**	25.5	**0.69**
A0-NP	37	40.2	1.04	19.5	**0.53**	23.4	**0.63**	44.0	**1.20**	25.5	**0.69**
A1-P-t8	46	44.0	0.96	24.4	**0.53**	21.1	**0.46**	48.4	1.06	28.5	**0.62**
A1-NP-t8	48	44.0	0.92	24.4	**0.51**	21.1	**0.44**	48.4	1.01	28.5	**0.59**
A2-P-t12	30	32.9	1.09	16.3	**0.54**	24.6	**0.82**	35.1	**1.17**	23.3	**0.77**
A2-NP-t12	31	32.9	1.06	16.3	**0.53**	24.6	**0.80**	35.1	**1.14**	23.3	**0.76**
A3-P-H70	69	74.7	1.08	42.5	**0.62**	28.6	**0.41**	75.6	1.10	31.0	**0.45**
A3-NP-H70	76	74.7	0.98	42.5	**0.56**	28.6	**0.38**	75.6	1.00	31.0	**0.41**
A4-P-H90	78	82.0	1.05	54.6	**0.70**	33.2	**0.42**	75.3	0.96	34.2	**0.44**
A4-NP-H90	80	82.0	1.02	54.6	**0.68**	33.2	**0.41**	75.3	0.94	34.2	**0.43**
A5-P-V70	44	43.3	0.98	21.7	**0.50**	23.4	**0.54**	41.8	0.96	25.5	**0.59**
A5-NP-V70	42	43.3	1.03	21.7	**0.52**	23.4	**0.56**	41.8	1.01	25.5	**0.61**
A6-P-V90	51	49.5	0.97	21.7	**0.42**	23.4	**0.46**	45.0	**0.88**	25.5	**0.50**
A6-NP-V90	51	49.5	0.97	21.7	**0.43**	23.4	**0.46**	45.0	**0.89**	25.5	**0.50**
A7-P-L50	48	45.2	0.94	19.5	**0.41**	23.4	**0.49**	48.8	1.02	25.5	**0.54**
A7-NP-L50	39	45.2	**1.15**	19.5	**0.49**	23.4	**0.59**	48.8	**1.24**	25.5	**0.65**
A8-P-L60	51	48.2	0.95	19.5	**0.38**	23.4	**0.46**	48.8	**0.89**	25.5	**0.50**

14

A8-NP-L60	47	48.2	1.03	19.5	**0.41**	23.4	**0.50**	48.8	1.03	25.5	**0.54**
A9-P-d24	37	37.2	1.01	19.5	**0.53**	23.4	**0.64**	47.1	**1.29**	25.5	**0.69**
A9-NP-d24	31	37.2	**1.20**	19.5	**0.64**	23.4	**0.76**	47.1	**1.54**	25.5	**0.83**

3.2. Bearing capacity

In EC3, angle in bending is regarded as an equivalent T-stub. As shown in Fig. 18, the resistance of T-stub in tension F_p can be derived as the smallest among three failure modes: T-stub complete yielded, bolt failure with yielded T-stub and bolt failure, as follows: Eqs. (10-12).

| (a) T-stub complete yielded | (b) Bolt fracture with yielded T-stub | (c) Bolt fracture |

Fig. 18 Failure modes of T-stub in tension
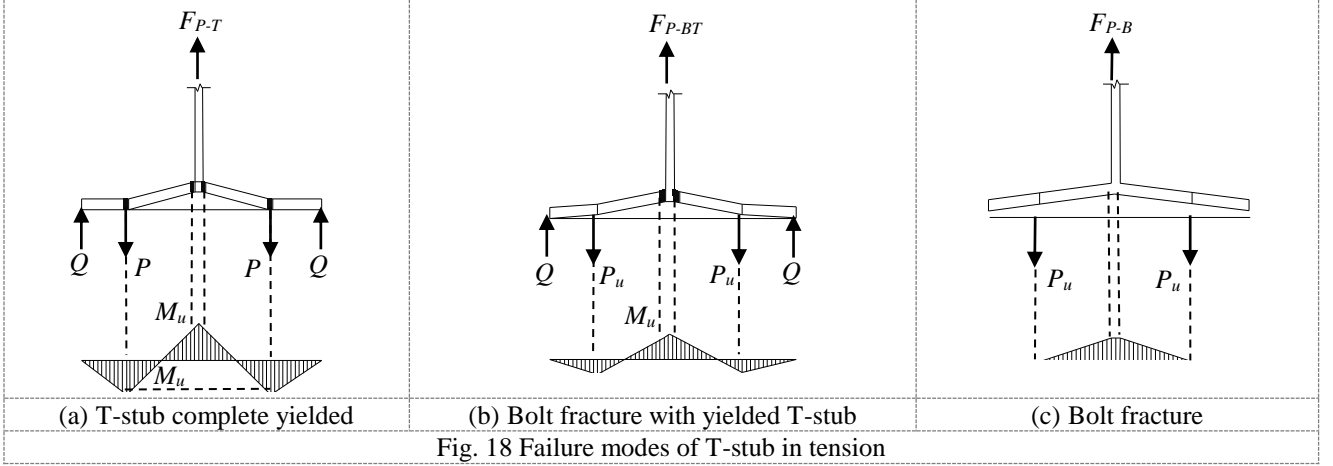
$$F_{p-T} = \frac{4M_a}{m_a} \tag{10}$$

where F_{p-T} is the design resistance of the connection with completely yielded T-stub. M_a is the plastic moment capacity of the T-stub flange, m_a is the distance between two plastic hinges. The criterion to calculate the value of m_a has been proposed in Eurocode 3-1-8 [31].

$$F_{p-BT} = \frac{2M_a + n_a \sum B_{T,Rd}}{m_a + n_a} \tag{11}$$

where F_{p-BT} is the design resistance of the failure mode with bolt fracture with yielded T-stub. n_a is the distance between the bolt center-lines and the prying force position. $B_{T,Rd}$ is the bolt design resistance.

$$F_{p-B} = \sum B_{T,Rd} \tag{12}$$

where F_{p-B} is the design resistance of the connection with bolt fracture.

The test results show that once the bolted angle connection enters the plastic deformation, the load displacement curve enters the nonlinear stage. Due to the tensile membrane action, the angle horizontal leg is gradually pulled up and the bolt yields or fractures. Meanwhile, a deformation gradually appeared between the vertical leg and the loading plate, as shown in Fig. 19.

Fig. 19 Deformation of vertical leg
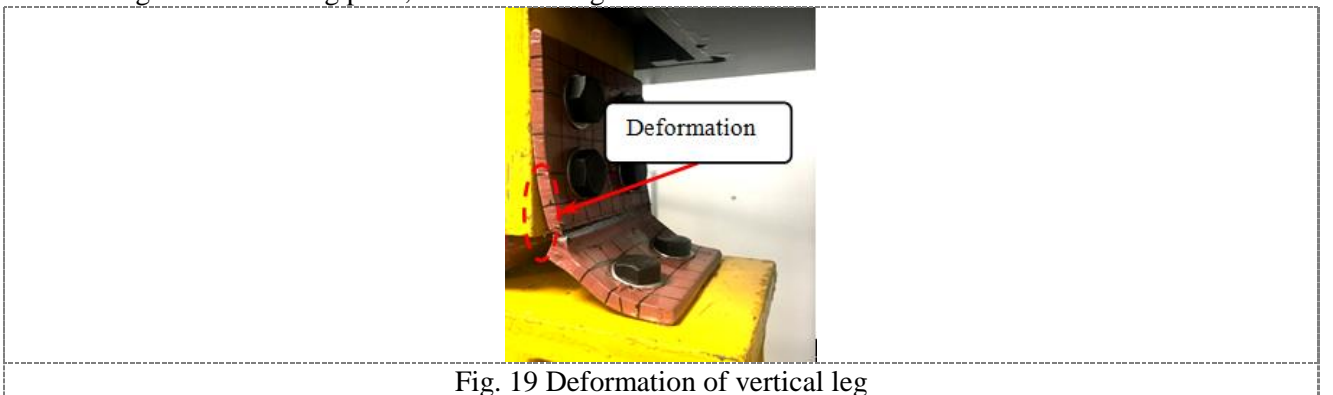
In view of the load increase gradually, Yang [39] proposed the incremental method to calculate the bearing capacity of the connection in the plastic deformation stage

$$F_{T,Y} = N_a + \Delta F \tag{13}$$

Eq. (9) is composed of N_a and ΔF parts, where N_a is the tension force of angle during the plastic deformation stage and ΔF is the load increment.

$$N_a = (b_{eff,a} - nd_{b,hole})tf_u \tag{14}$$

15

where $b_{eff,a}$ is the effective width of the bolted angles, n is the number of tension bolts and $d_{b,hole}$ is the bolt hole diameter.

$$\Delta F = F_2 - F_1 = N_a(sin\theta_2 - sin\theta_1)$$

$$= N_a(\frac{\Delta_1 + \delta}{\sqrt{g_H^2 + (\Delta_1 + \delta)^2}} - \frac{\Delta_1}{\sqrt{g_H^2 + \Delta_1^2}}) \qquad (15)$$

where displacement Δ is increased by a small amount δ in each step.

Gong [40] proposed two failure models (frame model and truss model) for the ultimate limit state of bolted angle connections. Frame model let angle legs being simulated as an elastic beam-column with plastic hinges at its ends, while truss model let the horizontal leg being seen as a pure tensile rode.

The calculation formula for the ultimate bearing capacity of bolted angle connection is obtained by using hermit cubic interpolation in frame model.

$$F_{u,frame-G} = k_T n N_a' \qquad (16)$$

where k_T is taken as 1.59, N_a' is the tension force of angle by the hermit cubic interpolation in literature [43].

The ultimate bearing capacity of the connection obtained by truss model is

$$F_{u,truss-G} = n[0.8 f_u t(b - d_{b,hole})]\frac{\Delta}{l_1} \qquad (17)$$

where b=76mm, Δ is the outstanding leg pulled away from the support, l_1 is the distance from the hinge at the bolt hole on the outstanding leg to the centerline of the vertical leg, $l_1 = g_H - t/2$.

Ref. [43] pointed out that the truss model was superior to the frame model and it has a much smaller coefficient of variation. Therefore, this paper only conducts validation analysis on the Truss Model. The comparison with test results in Table 5 shows that Eq. (13) overestimates the strength by 27.7% average and Eq. (17) underestimates the ultimate load by 17.7% average.

Through a regression analysis, a new formula for estimating the ultimate load of bolted angle connection based on Gong's model is proposed in this paper as

$$F_u = n[0.9 f_u t(\frac{1}{2}L_L - d_{b,hole})]\frac{\Delta}{g_H \varepsilon_u} \qquad (18)$$

The contribution of the vertical leg to the ultimate load is also considered in the calculation of ultimate load. The ultimate strength of net section is adopted in this formula with a calibration factor 0.9 to account for the actual tensile level, this is based on Gong's improvement [40]. More details regarding the mechanical model proposed by Gong are seen in Ref. [40]. Similar to the formula for the deformation capacity, more tested data are also needed to validate the proposed model, since some factors are derived through the regression analysis.

Table 5 Analysis of ultimate load

Specimen	Test	Proposed model		Shen and Astaneh-Asl		Yang's model		Gong's model	
	F_{u-t} /kN	F_{u-P} /kN	F_{u-P}/F_{u-t}	F_{u-Shen} /kN	F_{u-Shen}/F_{u-t}	F_{u-YT} /kN	F_{u-YT}/F_{u-t}	F_{u-G} /kN	F_{u-G}/F_{u-t}
A0-P	391	373	0.95	338	0.86	498	**1.27**	344	0.88
A0-NP	370	373	1.00	338	0.91	498	**1.35**	344	0.93
A1-P-t8	359	366	1.02	213	**0.59**	408	1.14	292	0.81
A1-NP-t8	362	382	1.05	213	**0.59**	408	1.13	292	0.81
A2-P-t12	468	432	0.92	372	**0.79**	509	1.09	376	0.80
A2-NP-t12	481	451	0.94	372	**0.77**	509	1.06	376	**0.78**
A3-P-H70	417	441	1.06	268	**0.64**	555	**1.33**	288	**0.69**
A3-NP-H70	438	476	1.09	268	**0.61**	555	**1.27**	288	**0.66**
A4-P-H90	426	441	1.07	254	**0.60**	483	1.13	242	**0.57**
A4-NP-H90	438	448	1.04	254	**0.58**	483	1.10	242	**0.55**
A5-P-V70	411	448	1.03	338	0.82	485	1.18	344	0.84
A5-NP-V70	430	428	0.98	338	**0.79**	485	1.13	344	0.80
A6-P-V90	436	448	0.99	338	**0.78**	505	1.16	344	**0.79**
A6-NP-V90	**336**	**448**	**1.15**	338	**0.78**	505	1.16	344	**0.79**
A7-P-L50	449	495	1.10	376	0.84	643	**1.43**	419	0.93
A7-NP-L50	391	413	1.06	376	0.96	643	**1.64**	419	1.07
A8-P-L60	458	487	1.06	418	0.91	758	**1.66**	494	1.08
A8-NP-L60	449	476	1.06	418	0.93	758	**1.69**	494	1.10
A9-P-d24	409	410	1.00	338	0.83	517	**1.26**	312	**0.76**

| A9-NP-d24 | 380 | 342 | 0.90 | 338 | 0.89 | 517 | **1.36** | 312 | 0.82 |

3.3. Initial stiffness

3.3.1 Angle in bending

The area contained in the center line of bolt holes is the effective bearing area of angle, as shown in Fig. 20. When the axial tension does not exceed the sum of bolt tensile strength P_u and friction force f, the rotation of the horizontal leg at the center line of the bolt holes is considered to be almost zero. As indicated in Fig. 21, take one half of angle for analysis.
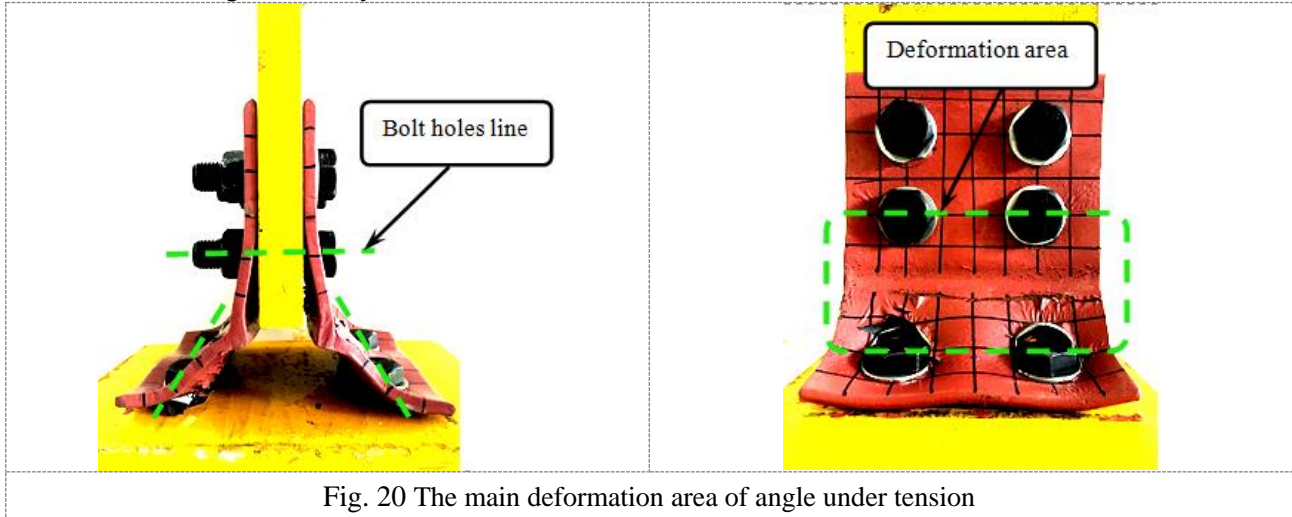

Fig. 20 The main deformation area of angle under tension

Fig. 21 shows a simplified model of angle. The stiffness of the loading device is large enough to the bolted angle connection and provides sufficient restraint for the horizontal leg. Plate A is equivalent to a quarter of the plate subject to the concentrated load with two fixed opposite sides and two rotation-restrained opposite sides. Therefore, it is assumed that edge 12 is a fixed edge and the remaining three edges are subject to rotation-restrained. The deflection at point 1 is obtained by the rectangular plate under the central concentrated load P.
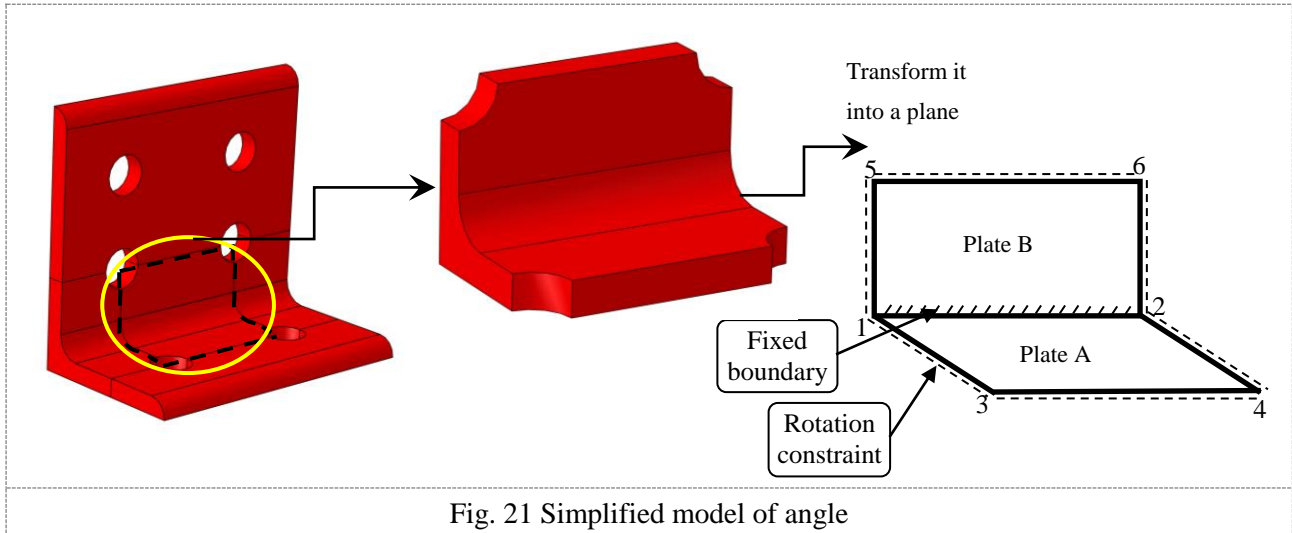

Fig. 21 Simplified model of angle

When concentrated load P acts on the center of the rectangular plate, its deflection is [44]:

$$w_m = \frac{\alpha P a^2}{D} \tag{19}$$

where $D=Et^3/12(1-v^2)$ is the flexural deflection of a unit rectangular plate; v is the Poisson's ratio; a is the length of the rectangle; α is the coefficient related to the side length ratio and constraint conditions of the rectangular plate.

For a rectangular plate with a pair of fixed constraints and a pair of rotating constraints, the α is calculated by the following [44]:

$$\alpha_1 = f(\lambda) = \begin{cases} 0.0084\lambda^{-0.732} & (\lambda \leq 0.87) \\ 0.0093 & (\lambda > 0.87) \end{cases} \tag{20}$$

17

where $\lambda = b/a$ is the edge length ratio, b is the length of the fixed edge.

Thus, the deflection of plate A at point 1 can be obtained through Eq. (19) and (20) [44]:

$$w_{Plate1} = \frac{P_1}{k_{ep1}} \tag{21}$$

where $k_{ep1} = \frac{D}{16\alpha_1 g_L^2} = \frac{Et^3}{48(1-v^2)F_1(g_H,g_L)}$; P_1 is the load on point 1.

F_1 is given by the following:

$$F_1(g_H,g_L) = \begin{cases} 0.336(2g_L)^2(\frac{g_H}{2g_L})^{-0.732} & \lambda \leq 0.87 \\ 0.0372(2g_L)^2 & \lambda > 0.87 \end{cases} \tag{22}$$

The deflection of Plate B can still be calculated by Eq. (19). α is calculated by the following [45]:

$$\alpha_2 = f(\lambda) = \frac{0.00725}{(1+4\lambda^{-7}+\lambda^{-14})^{1/7}} \tag{23}$$

Like Plate A, the deflection of plate B at point 2 is:

$$w_{Plate2} = \frac{P_2}{k_{ep2}} \tag{24}$$

$$k_{ep2} = \frac{D}{16\alpha_2 g_L^2} = \frac{Et^3}{48(1-v^2)F_2(g_H,g_L)} \tag{25}$$

$$F_2(g_H,g_L) = 4f_2(\frac{g_H}{2g_L})(2g_L)^2 = \frac{0.029g_H^2(2g_L)^2}{[g_H^{14}+(2g_L)^2+4g_H^7(2g_L)^2]^{1/7}} \tag{26}$$

3.3.2 Bolt in tension

In Ref. [46-47], the stiffness of bolt is generally calculated by the following formula

$$k_{bt-NP} = 1.6\frac{EA_b}{L_b} \tag{27}$$

where A_b is the effective area of the bolt; the effective length of the bolt $L_b=t_{ep}+t+2t_c+(h_1+h_2)/2$, according to EC3; h_1 and h_2 are the thickness of the bolt head and nut respectively; t_c is the thickness of the washer; t_{ep} is the thickness of the loading device.

The coefficient 1.6 is used to consider the increase of the bolt tension due to prying force. If the effect of prying force is not considered, the coefficient is 2.0. The tensile deformation of the bolt is controlled only by the stiffness of the bolt itself in the connections without bolt preload. Therefore, the tensile stiffness of bolts without preload is calculated by Eq. (27).

The reason for the significant increase in the initial stiffness of the connection is that the bolt and the plate around the bolt hole work as a whole and bear tensile load together.

Therefore, the stiffness of the bolt after applying the preload is controlled by the sum of the two [48-49]

$$k_{bp} = k_b + k_p \tag{28}$$

where k_{bp} is the stiffness of the bolt-plate, k_b is the axial stiffness of a single bolt, k_p is the stiffness contribution of the connected plate, whose can be calculated by the following formula in Ref. [50]

$$\frac{k_p}{k_b} = 4.10 + 3.25\frac{t_{ep}+t}{d_b} \tag{29}$$

To sum up, the tensile stiffness of bolt with preload can be calculated by the following

$$k_{bt-P} = 2(5.10 + 3.25\frac{t_{ep}+t}{d_b})\frac{EA_b}{L_b} \tag{30}$$

3.3.3 Stiffness integration of connection

The stiffness of the connection is controlled by both bolts and angle. If k_1 and k_2 are respectively the stiffness of Plate A and Plate B, then:

$$k_1 = \frac{P_1}{\Delta_1}; \ k_2 = \frac{P_2}{\Delta_2} \tag{31}$$

where Δ_1 and Δ_2 are the total deformation at point 1 and 2 respectively, which can be obtained by the following

$$k_1 = \cfrac{1}{\cfrac{1}{k_{ep1}} + \cfrac{1}{k_{bt}}} \; ; \quad k_2 = \cfrac{1}{\cfrac{1}{k_{ep2}} + \cfrac{1}{k_{bt}}} \tag{32}$$

When the connection with bolt preload, Eq. (32) can be expressed as

$$k_{1-P} = \cfrac{1}{\cfrac{1}{k_{ep1}} + \cfrac{1}{k_{bt-P}}} \; ; \quad k_{2-P} = \cfrac{1}{\cfrac{1}{k_{ep2}} + \cfrac{1}{k_{bt-P}}} \tag{33}$$

When the connection without bolt preload, Eq. (32) can be expressed as:

$$k_{1-NP} = \cfrac{1}{\cfrac{1}{k_{ep1}} + \cfrac{1}{k_{bt-NP}}} \; ; \quad k_{2-NP} = \cfrac{1}{\cfrac{1}{k_{ep2}} + \cfrac{1}{k_{bt-NP}}} \tag{34}$$

Based on the test results, a calculation method for the initial stiffness of bolted angle connection is proposed

$$k_{con-P} = 2\left[\frac{2g_L g_H}{(L_H - t_{vd})L_L} k_{1-P} + \frac{(L_H - t_{vd} - 2g_H)/2}{L_H} k_{2-P}\right] \tag{35}$$

$$k_{con-NP} = 2\left[\frac{2g_L g_H}{(L_H - t_{vd})L_L} k_{1-NP} + \frac{(L_H - t_{vd} - 2g_H)/2}{L_H} k_{2-NP}\right] \tag{36}$$

where k_{con-P} stands for the initial stiffness of the connection with bolt preload; k_{con-NP} stands for the initial stiffness of the connection without bolt preload; t_{vd} is the thickness of the vertical plate, which was t_{vd}=25mm.

In Table 6, the predicted value of bolted angle connection and the calculated value using EC3 are given and compared with the experimental value. It can be seen that the results obtained by using the calculation method presented in this paper are in good agreement with the experimental results.

Table 6 Comparison of the predicted and tested initial stiffness

Specimen No.	Test (kN/mm)	Eq. (35-36) (kN/mm)	Eq. (35-36)/Test	EC3 (kN/mm)	EC3/Test
A0-P	38	39	1.03	25	0.66
A0-NP	20	22	1.10	25	1.25
A1-P-t8	35	37	1.06	27	0.77
A1-NP-t8	19	18	0.95	27	1.42
A2-P-t12	33	32	0.97	25	0.76
A2-NP-t12	23	25	1.09	25	1.09
A3-P-H70	14	15	1.07	20	1.43
A3-NP-H70	11	10	0.91	20	0.91
A4-P-H90	11	12	1.09	16	1.45
A4-NP-H90	9	11	1.22	16	1.78
A5-P-V70	22	24	1.10	25	1.14
A5-NP-V70	21	23	1.10	25	1.19
A6-P-V90	19	20	1.05	25	1.32
A6-NP-V90	17	16	0.94	25	1.47
A7-P-L50	39	41	1.05	25	0.64
A7-NP-L50	21	20	0.95	25	1.19
A8-P-L60	41	39	0.95	25	0.61
A8-NP-L60	24	25	1.04	25	1.04
A9-P-d24	32	33	1.03	40	1.25
A9-NP-d24	28	30	1.07	40	1.43

4. Mechanical model of the connection

4.1. Model development

A load-displacement relationship model is developed based on Eurocode Component Method to describe the entire deformation process of bolted angle connections under tension, as shown in Fig. 22. F_u and Δ_u is the ultimate load and ultimate deformation of the bolted angle connection respectively. The value of Δ_u can be

derived in Section 3.1. F_u can be already found in Section 3.2. F_p is the plastic strength, which is calculated by using the elastic-plastic model in Eurocode 3-1-8 [31] as described in detail in Section 3.2. The value of yield strength F_y was recommended to be 2/3 F_p [39].
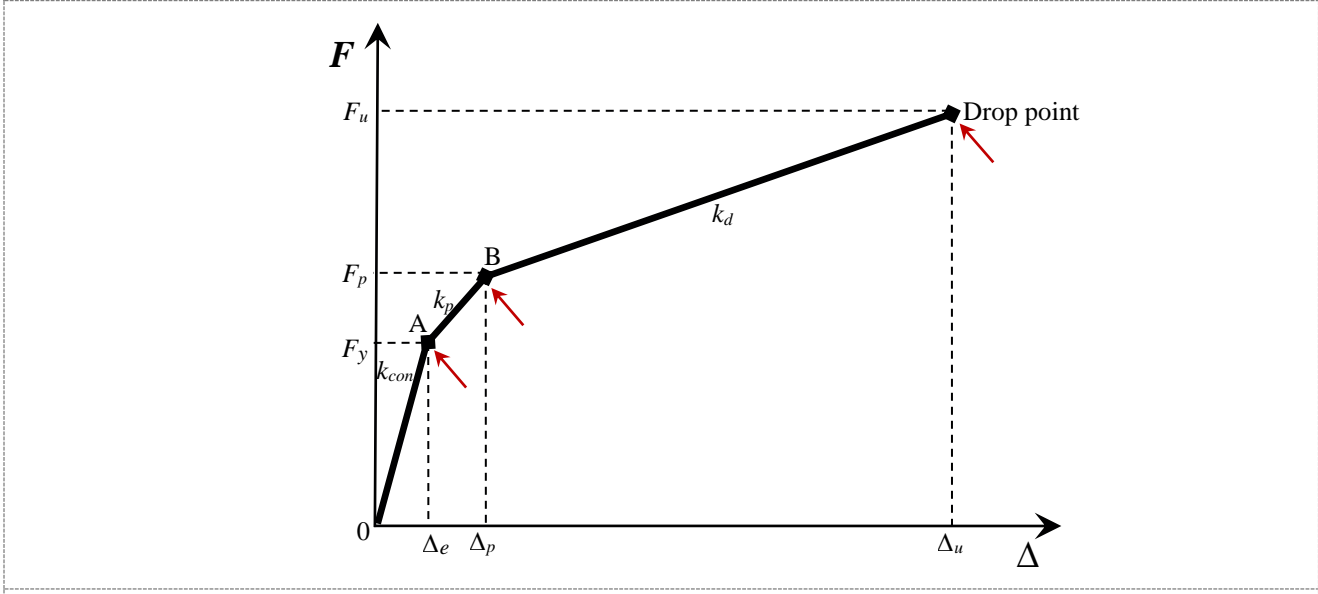

Fig. 22 Mechanical model of the displacement-load curve for bolted angle connections

The bolt hole diameter is 2mm larger than the bolt shank diameter and the bolt slip will occurred theoretically during the experiment. When the shear force is less than the friction force, the stiffness of the connection is large. Once the shear force overcomes the friction force, the stiffness is reduced to zero. However, when the gap between the bolt shanks and the holes is closed, the stiffness will be large once again. However, from the experimental load-displacement curve, there is no obvious bolt slip, so the bolt slip stage is not considered in the proposed model.

The initial stiffness in the model involves k_{con-P} and k_{con-NP} due to the influence of bolt preload, as described in Eqs. (17) and (18). The value of k_p was recommended to be $1/7k_{con}$ [50]. k_d can be calculated by ultimate load and ultimate displacement.

In Fig. 22, there are three key points A, B and drop point in the load-displacement curve of the mechanical model. Section 0-A is the elastic section of the curve. At this stage, the initial stiffness k_{con} and the yield strength F_y of the connection can be obtained. The yield strength F_y is 2/3 of the plastic strength F_p. The initial stiffness is obtained from Eqs. (35) and (36). Section A-B is the plastic stage of the load-displacement curve. The coordinate corresponding to the key point B is (Δ_P, F_p). The point coordinates of point B can be determined by the slope k_p of AB and plastic strength F_p. The value of k_p was recommended to be $1/7k_{con}$. The F_p is the plastic strength, which is calculated using Eqs. (10-12). After the curve exceeds point B, it enters into the plastic deformation stage, until the bolted angle connection is fractured and the load displacement curve reaches drop point. Drop point corresponds to the ultimate deformation Δ_u and ultimate load F_u of the connection. Δ_u and F_u are obtained from Eqs. (8) and (18) respectively. The proposed model is summarized in Table 7 for better understanding.

Table 7 Summarization of the proposed model

Key point	Abscissa	Ordinate
	Δ_e	F_y
A	$$\Delta_e = \frac{F_y}{k_{con}}$$ $$k_{con-P} = 2[\frac{2g_L g_H}{(L_H - t_{vd})L_L}k_{1-P} + \frac{(L_H - t_{vd} - 2g_H)/2}{L_H}k_{2-P}]$$ for the bolts with pretension $$k_{con-NP} = 2[\frac{2g_L g_H}{(L_H - t_{vd})L_L}k_{1-NP} + \frac{(L_H - t_{vd} - 2g_H)/2}{L_H}k_{2-NP}]$$ for the bolts without pretension	$F_y = 2/3F_p$
B	Δ_p	F_p

20

$$\Delta_p = \frac{F_p - F_y + 1/7 k_{con} \Delta_e}{1/7 k_{con}}$$

$$F_{p-T} = \frac{4M_a}{m_a}$$

for the connection with completely yielded T-stub

$$F_{p-BT} = \frac{2M_a + n_a \sum B_{T,Rd}}{m_a + n_a}$$

for the failure mode with bolt fracture with yielded T-stub

$$F_{p-B} = \sum B_{T,Rd}$$

for the connection with bolt fracture

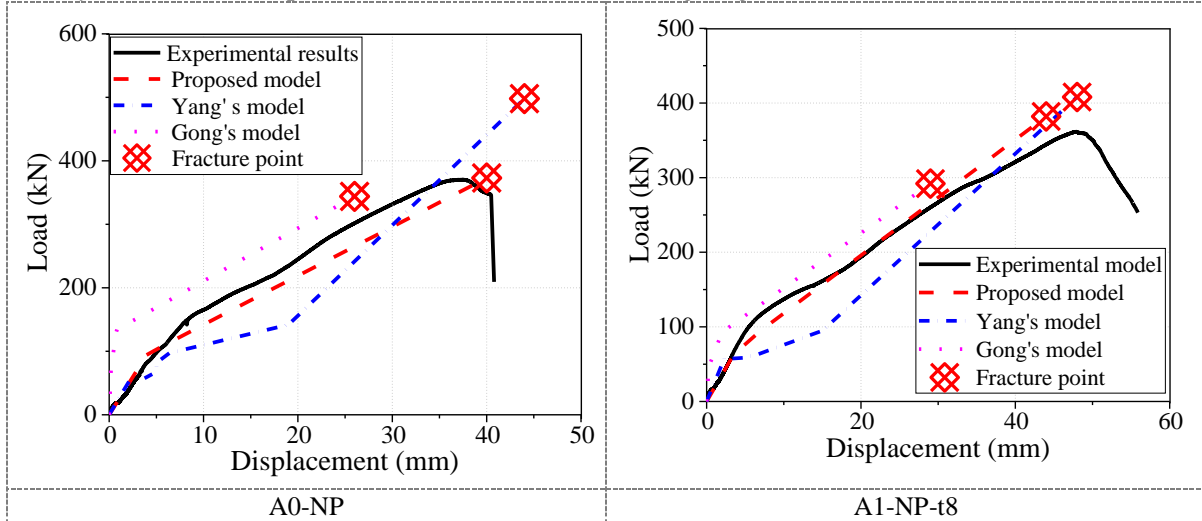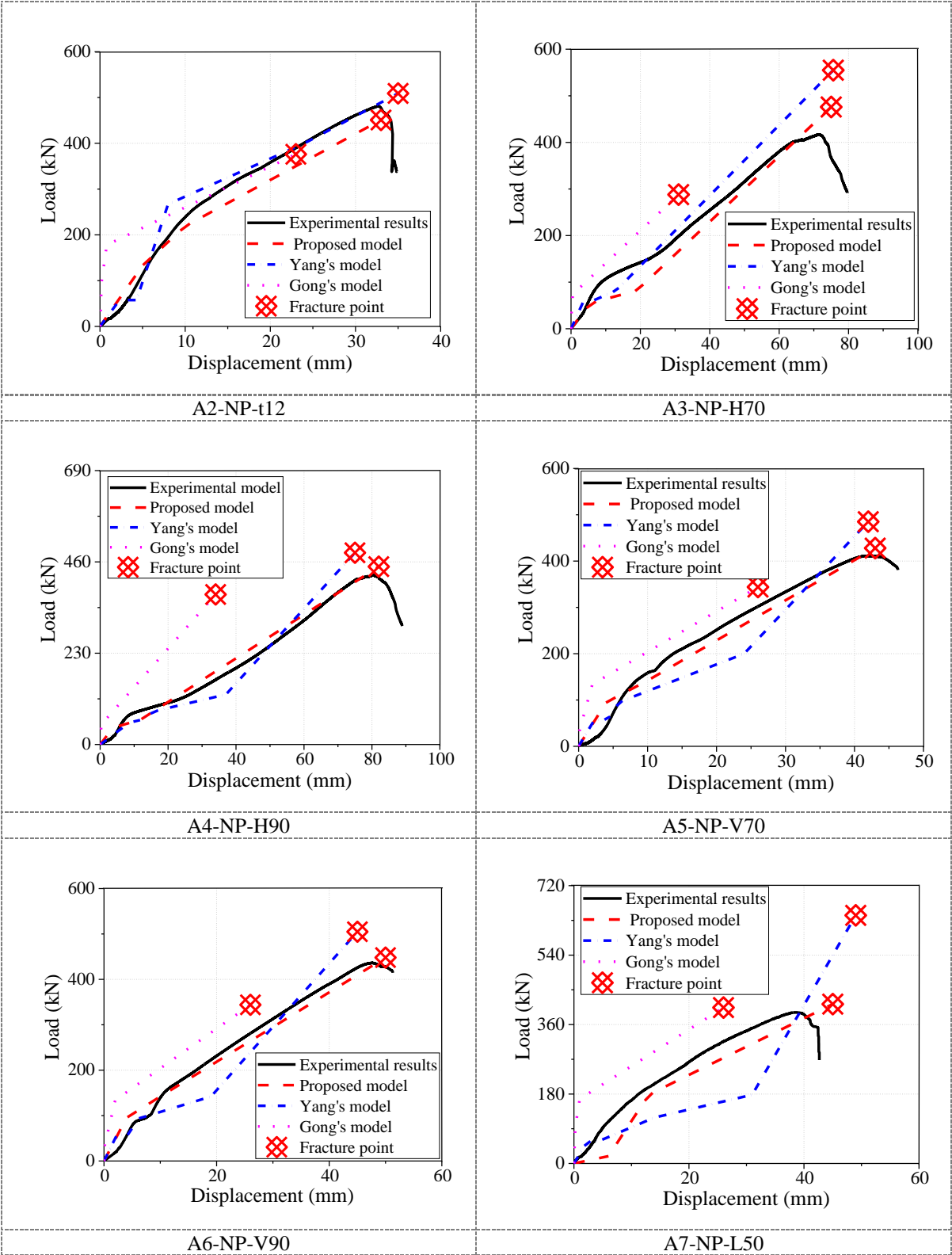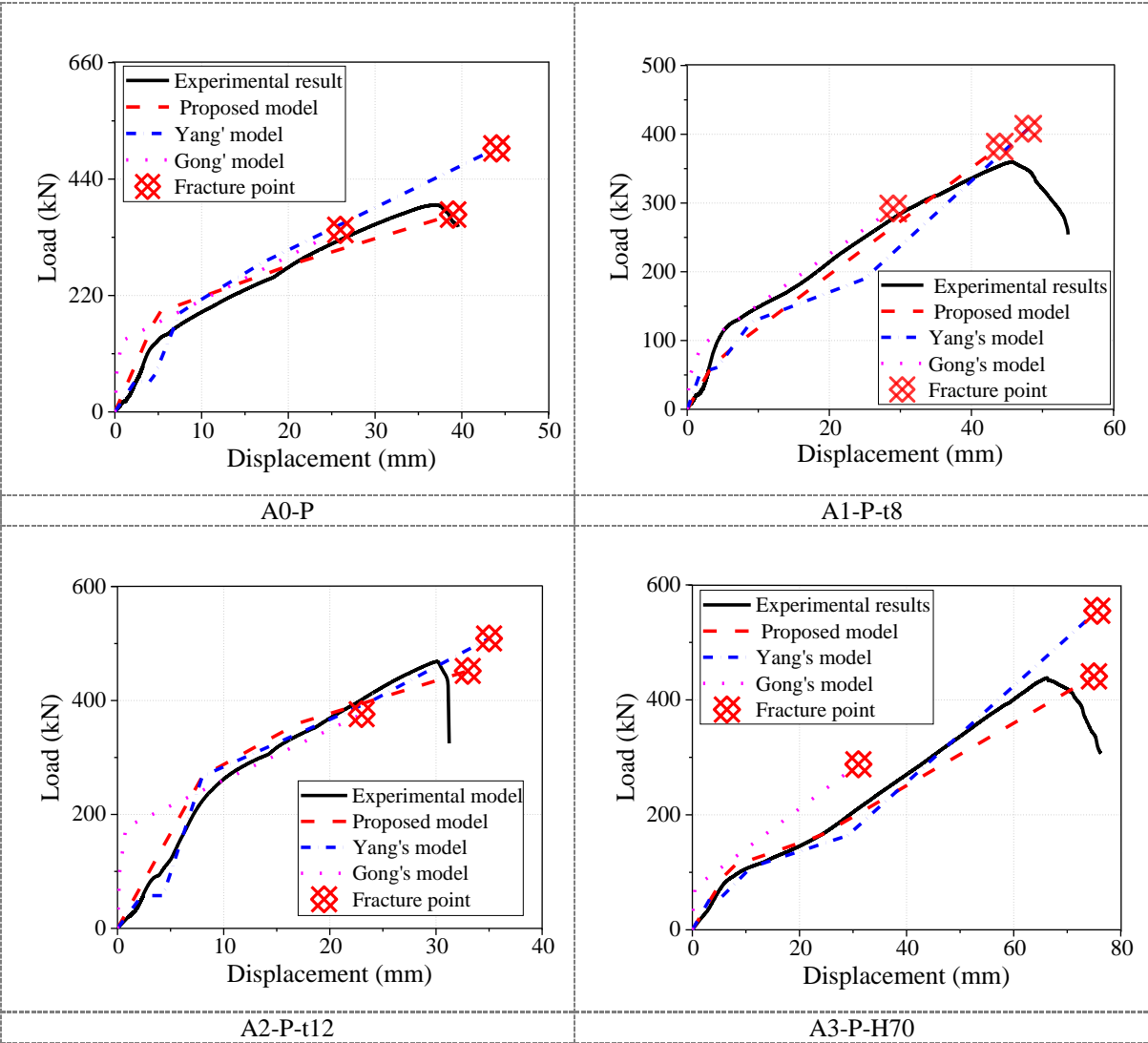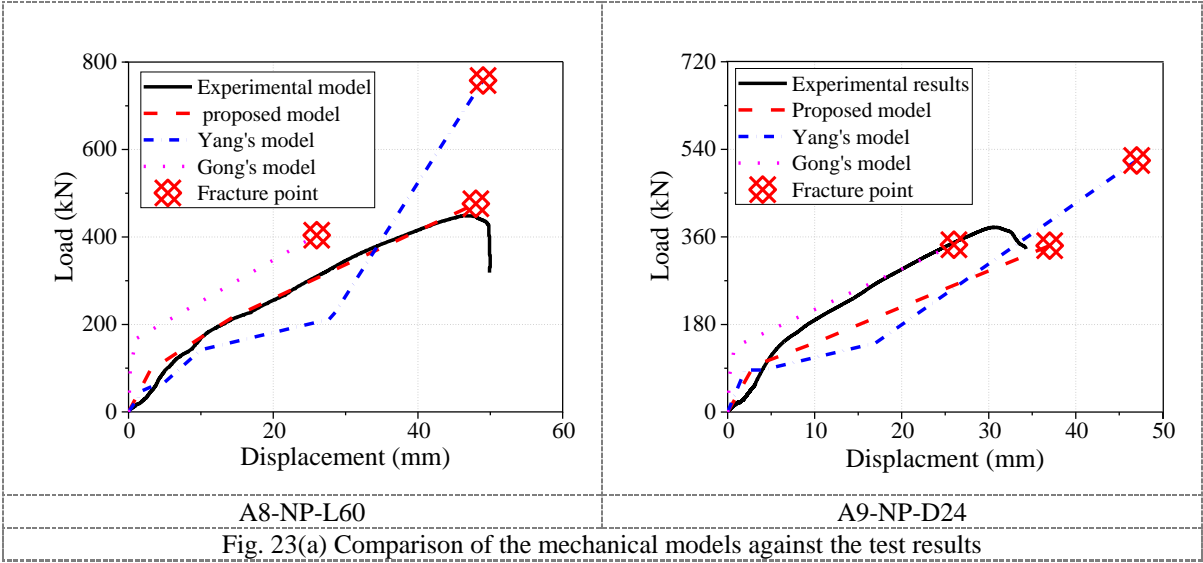|	Δ_u	F_u
Drop point	$\Delta u = \sqrt{g_H^{*2} + g_V^{*2}}(1+\varepsilon_u)\sin\theta$ $g_H^{*} = g_H - t - 0.8r_a + \eta d_b$ $g_V^{*} = g_V - t - 0.8r_a + \eta d_b$	$F_u = n[0.9 f_u t (\frac{1}{2} L_L - d_{b,hole})]\frac{\Delta}{g_H \varepsilon_u}$

4.2. Validation of the mechanical model

The predicted results from the proposed mechanical model are compared with the experimental results, as shown in Fig. 23. It can be seen that the predicted values of the proposed model are in good agreement with test results. To further verify the validity and accuracy of the proposed model, the prediction curves of Yang's model and Gong's model are also shown in Fig. 23.

The proposed model is better than the Gong's model in initial stiffness, while the model proposed by Gong also shows large difference in ultimate load and ultimate deformation. From the curve trend, the predicted curve of Yang's model differs greatly from the experimental results at a certain stage. At the same time, bolt slippage was considered in Yang's model, but from the experimental curve, the bolt slip stage was not obvious, which may be due to the slip at the chuck at the initial loading stage.

A0-NP

A1-NP-t8

A2-NP-t12

A3-NP-H70

A4-NP-H90

A5-NP-V70

A6-NP-V90

A7-NP-L50

A8-NP-L60

A9-NP-D24

Fig. 23(a) Comparison of the mechanical models against the test results

A0-P

A1-P-t8

A2-P-t12

A3-P-H70

A4-P-H90

A5-P-V70

A6-P-V90

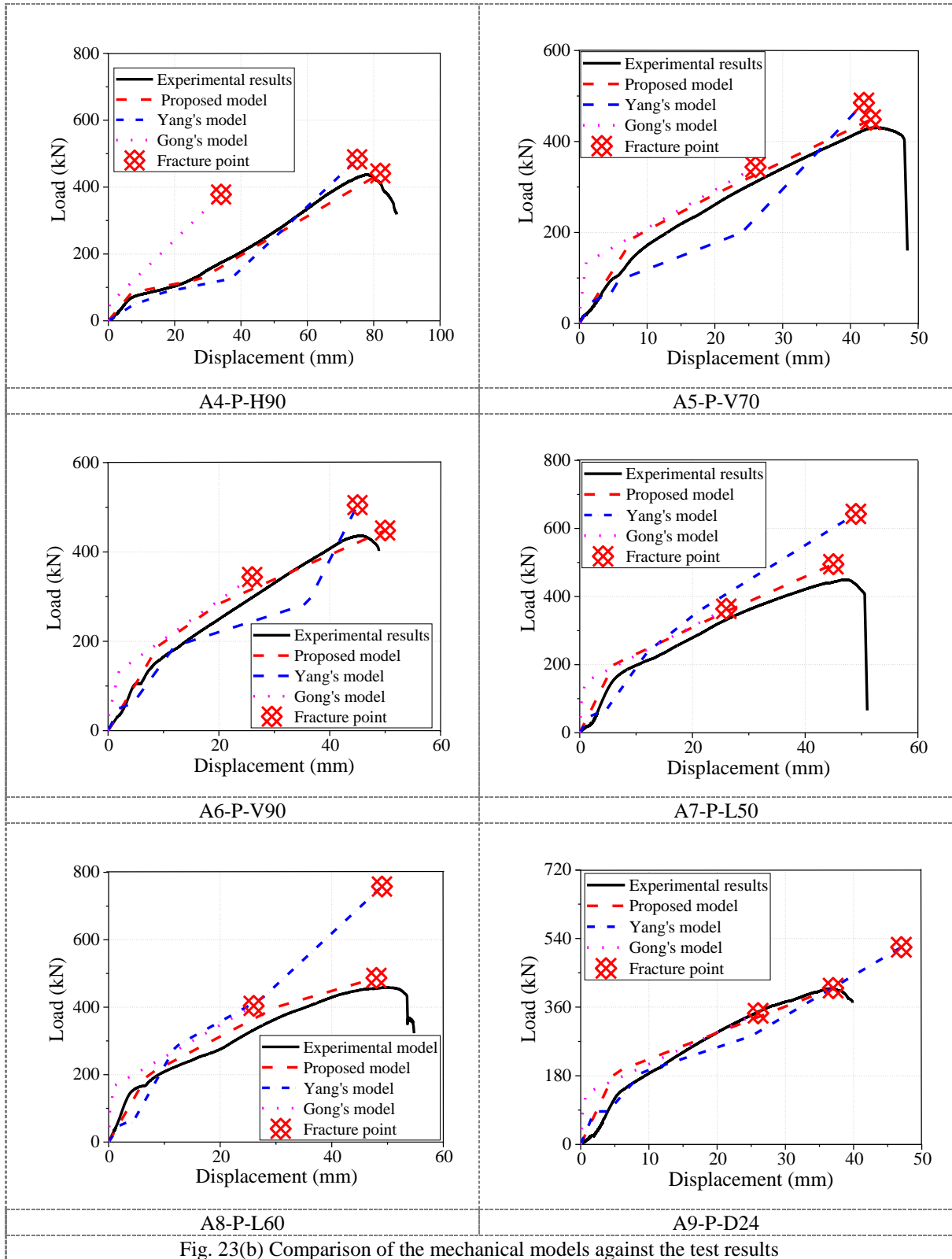A7-P-L50

A8-P-L60

A9-P-D24

Fig. 23(b) Comparison of the mechanical models against the test results

5. Conclusions

This paper aims to investigate the ultimate tensile behavior of bolted angle connections. Six design parameters of the connection were considered in the experiment, including angle thickness t, horizontal bolt pitch g_H, vertical bolt pitch g_V, longitudinal bolt pitch g_L, bolt diameter d and bolt preload P. The experimental phenomena and results are discussed in detail. A mechanical model of bolted angle connections is developed according to the test results. Below conclusions can be drawn:

1) Under the monotonic tension, bolted angle connection showed five kinds of failure modes, namely angle fracture at heel (A0, A7, A8, A9), angle fracture at bolt holes line (A1), bolt fracture with yielded angle (A2), angle fracture at bolt holes line with yielded bolt (A3, A4) and angle fracture close to heel (A5, A6).

2) By analyzing the mechanical properties of bolted angle connections under different parameters, it can be seen that angle thickness t and vertical bolt pitch g_V are positively correlated with the ultimate bearing capacity of connections, but negatively correlated with ultimate deformation of the connection. However, with the increase of horizontal bolt pitch g_H and longitudinal bolt pitch g_L, the ultimate load of the connection gradually is strengthened and the ultimate deformation gradually increases. In the elastic stage of load-displacement curve, the bearing capacity of the specimens with bolt preload is higher than that of the specimens without bolt preload.

3) The experimental results show that both horizontal leg and vertical leg contribute to the deformation of the connection. Therefore, by considering the influence of the horizontal leg and vertical leg on the ultimate deformation of the connection, a formula for calculating the ultimate deformation of the bolted angle connection is proposed and validated against the test results.

4) An improved formula is proposed to predict the tensile capacities of bolted angle connections. The predicted results agree with the tested values better than other formulas. Using the theory of plate-shell, the formulas for calculating the initial stiffness of the connections with or without bolt preload are derived respectively. By comparing with EC3, the validity and accuracy of the formula proposed in this paper are verified.

5) A mechanical model is proposed and used to predict the load-displacement curve of bolted angle connection, which is also compared with Yang's model and Gong's model. The proposed model fits best with the tested results among all the considered models.

Acknowledgements

References

[1] Marjanishvili S, Agnew E. Comparison of various procedures for progressive collapse analysis. Journal of Performance of Constructed Facilities, 2006, 20(4): 365-374.

[2] Liu M. A new dynamic increase factor for nonlinear static alternate path analysis of building frames against progressive collapse. Engineering structures, 2013, 48: 666-673.

[3] Brunesi E., Nascimbene R., Parisi F., et al. Progressive collapse fragility of reinforced concrete framed structures through incremental dynamic analysis. Engineering Structures, 104: 65-79.

[4] Kokot S, Anthoine A, Negro P, et al. Static and dynamic analysis of a reinforced concrete flat slab frame building for progressive collapse. Engineering Structures, 2012, 40: 205-217.

[5] Stinger S M, Orton S L. Experimental evaluation of disproportionate collapse resistance in reinforced concrete frames. ACI Structural journal, 2013, 110(3).

[6] Brunesi E., Nascimbene R. Extreme response of reinforced concrete buildings through fiber force-based finite element analysis. Engineering Structures. 2014, 69: 206-215.

[7] Ravasini S., Belletti B., Brunesi E., et al. Nonlinear dynamic response of a precast concrete building to sudden column removal. Applied Sciences. 2021, 11, 599.

[8] Chen J, Huang X, Ma R, et al. Experimental study on the progressive collapse resistance of a two-story steel moment frame. Journal of Performance of Constructed Facilities, 2011, 26(5): 567-575.

[9] Naji A, Irani F. Progressive collapse analysis of steel frames: Simplified procedure and explicit expression for dynamic increase factor. International Journal of Steel Structures, 2012, 12(4): 537-549.

[10] Li H.H., Cai X.H., Zhang L. et al. Progressive collapse of steel moment-resisting frame subjected to loss of interior column: Experimental tests. Engineering Structures, 2017, 150: 203-220.

[11] Rodriguez D, Brunesi E, Nascimbene R. Fragility and sensitivity analysis of steel frames with bolted-angle connections under progressive collapse. Engineering Structures. 2021, 228, 111508.

[12] Wang W.D., Li H.W., Wang J.X. Progressive collapse analysis of concrete-filled steel tubular column to steel beam connections using multi-scale model. Structures, 2017, 9: 123-133.

[13] Gao S., Xu M., Zhang S.M. Dynamic analysis of CFST composite frame against progressive collapse based on Benchmark model. Advances in Structural Engineering. 2018, 21(7): 1021-1035.

[14] Gao S. Nonlinear finite element failure analysis of bolted steel-concrete composite frame under column-loss. Journal of Constructional Steel Research, 2019, 155: 62-76.

[15] Qin W.H., Liu X.Y., Xi Z., et al. Experimental research on the progressive collapse resistance of concrete beam-column sub-assemblages reinforced with steel-FRP composite bar. Engineering Structures. 2021, 111776.

[16] BS8110-1:1997. Structural Use of Concrete: Part 1: Code of Practice for Design and Construction. British Standard Institute, 2002.

[17] Draft prEN 1991-1-7, Eurocode 1-Actions on Structures, Part 1-7: General Actions - Accidental Aactions. Brussels: European Committee for Standardization, 2005.

[18] National Building Code of Canada. National Research Council of Canada, Ottawa. Canada, 1975.

[19] United States General Services Administration (GSA). Progressive collapse analysis and design guidelines for new federal office buildings and major modernization projects. Washington (DC). 2003.

[20] U.S. Department of Defense. Unified Facilities Criteria: Design of Building to Resist Progressive Collapse. UFC 4-023-03, USA, 2013.

[21] Oosterhof S.A., Driver R.G. Performance of steel shear connections under combined moment, shear, and tension. Structures Congress 2012. 2012: 146-157.

[22] Daneshvar H., Driver R.G. Behaviour of single angle connections under simultaneous shear, tension and moment. Structures. 2018, 15: 13-27.

[23] Shen J., Astaneh-Asl A. Hysteretic behavior of bolted-angle connections. Journal of Constructional Steel Research. 1999, 51: 201-218.

[24] Shen J., Astaneh-Asl A. Hysteresis model of bolted-angle connections. Journal of Constructional Steel Research. 2000, 54: 317-343.

[25] Beland T., Bradley C. R., Nelson J., et al. Experimental parametric characterization of bolted angle connection behavior. Journal of Structural Engineering. 2020, 146(8):1-7.

[26] Yang B., Tan K.H. Robustness of bolted-angle connections against progressive collapse: Experimental tests of beam-column joints and development of component-based models. Journal of Structural Engineering, 2012, 139(9): 1498-1514.

[27] Weigand J.M., Berman J.W. Integrity of bolted angle connections subjected to simulated column removal. Journal of Structural Engineering, 2016, 142(3): 04015165.

[28] Oosterhof S.A, Driver R.G. Behavior of steel shear connections under column-removal demands. Journal of Structural Engineering, 2014, 141(4): 04014126.

[29] Oosterhof S.A, Driver R.G. Shear connection modelling for column removal analysis. Journal of Constructional Steel Research, 2016, 117:227-242.

[30] Gong Y L. Test, modeling and design of bolted-angle connections subjected to column removal. Journal of Constructional Steel Research, 2017, 139:315-326.

[31] EN1993-1-8. Eurocode 3: Design of Steel Structures Part 1-8: Design of joints. Brussels, European Committee for standardization, 2005.

[32] Anwar GA, Dinu F, Ahmed M. Numerical study on ultimate deformation and resistance capacity of bolted T-stub connection. International Journal of Steel Structures. 2019, 19: 970-977.

[33] Bao W., Jiang J., Yu Z.W., et al. Mechanical behavior of high-strength bolts in T-stubs based on moment distribution. Engineering Structures. 2019, 196, 109334.

[34] Godrich L., Wald F., Kabelac J., et al. Design finite element model of a bolted T-stub connection component. Journal of Structural Engineering. 2019, 157: 198-206.

[35] Tartaglia R, D'Aniello M, Zimbru M. Experimental and numerical study on the T-Stub behaviour with preloaded bolts under large deformations. Structures. 2020, 27: 2137-2155.

[36] Bezerra L.M., Bonilla J., Silva W.A., et al. Experimental and numerical studies of bolted T-stub steel connection with different flange thicknesses connected to a rigid base. Engineering Structures. 2020, 218, 110770.

[37] Izzuddin B.A., Vlassis A.G., Nethercot D.A. Progressive collapse of multi-storey buildings due to sudden column loss-part i: simplified assessment framework. Engineering Structures, 2008, 30(5): 1308-1318.

[38] Guo L.H., Gao S., Fu F., et al. Experimental study and numerical analysis of progressive collapse resistance of composite frames. Jounal of Constructional Steel Research. 2013, 89: 236-251.

[39] Yang B, Tan K H. Robustness of bolted-angle connections against progressive collapse: Mechanical modelling of bolted-angle connections under tension. Engineering Structures, 2013, 57(4):153-168.

[40] Gong Y L. Ultimate tensile deformation and strength capacities of bolted-angle connections. Journal of Constructional Steel Research, 2014, 100:50-59.

[41] Piluso V, Faella C, Rizzano G. Ultimate behaviour of bolted T-stubs. II: Model validation. Journal of Structural Engeering, ASCE 2001; 127(6): 694-704.

[42] BCSA/SCI. Joints in steel construction-simple connections. Steel Construction Institute, Ascot; 2002.

[43] Taranath BS. Steel concrete composite design of tall Buildings, second edition, McGraw-Hill, 965-975.

[44] Wu Z.Q. Beam-to-column bolted extended endplate connection and its influence on frame behavior. PhD Thesis, Harbin Institute of Technology, 2008.

[45] Guo B., Gu Q. Experimental study on hysteretic behavior of beam-column end-plate connection joints. Journal of Building Structures, 2002, 23(3): 8-13.

[46] Fisher, J W, Struik S H A. Guide to design Criteria for bolted and riveted joints, Wiley, 1974.

[47] Yee Y L, Melchers R E. Moment-rotation curves for bolted connections. Journal of Structural Engineering, 1986, 112(3): 615-635.

[48] Foley C M, Vinnakota S. Toward design office moment-rotation curves for end-plate beam-to-column connections. Journal of Constructional Steel Research, 1995, 35(2): 217-253.

[49] Summer EA. Unified Design Extended End-plate Moment Connection Subject to Cycle Loading, PhD Thesis, The Virginia Polytechnic Institute and State University, 2003.

[50] Faella C, Piluso V, Rizzano G. Structural steel semirigid connections: theory, design and software. In: New directions in civil engineering. Boca Raton (FL (EEUU)): CRC Publishers; 2000.